Divergent T cell programs in plaque rupture and erosion revealed by single-cell multiomics in the OPTICO-ACS study

Hauke Horstmann[1,2*], Christopher Wolfram[3,4*], Lauren De Vore[5,6], Youssef S. Abdelwahed[7,8], Anaïs Amend[1], Denitsa Meteva[7,8], Merlin Heiser[7,8], Philip Stapmanns[7,9], Claudio Seppelt[3,4], Lukas Zanders[3,4], Gregor Nelles[3,4], David Peters[5,6], Chantal Wientjens[5,6], Florian Zimmermann[5,6], Deniz Yücel[5,6], Marek Franitza[6,10], Kerstin Becker[6,10], Corinna Losert[11,12], Matthias Heinig[11,12,13], Konstantin Stark[13,14], Michael Joner[14,15], Alexander Lang[16], Thomas Riffelmacher[5,6], Norbert Gerdes[16,17], Stephan Baldus[5,6], Chiara Giannarelli[1], Dennis Wolf[2], Ulf Landmesser[7,8], Nicolle Kränkel[7,8], David M. Leistner[3,4], Holger Winkels[5,6**], Teresa Gerhardt[4,18,19**]

1. New York University Cardiovascular Research Center, New York University Langone Health, New York, NY, USA.
2. Department of Cardiology and Angiology I, Medical Center, University of Freiburg, Germany.
3. Department of Medicine, Cardiology/Angiology, Goethe University Hospital, Frankfurt, Germany.
4. DZHK (German Centre for Cardiovascular Research), partner site Frankfurt Rhine-Main, Frankfurt, Germany.
5. Department of Cardiology, Heart Center, Faculty of Medicine, University of Cologne, Cologne, Germany; Center for Cardiovascular Medicine ABCD, Aachen - Bonn - Cologne - Düsseldorf, Germany.
6. Center for Molecular Medicine Cologne, University of Cologne, Cologne, Germany.
7. Department of Cardiology, Angiology and Intensive Care Medicine, Deutsches Herzzentrum der Charité (DHZC), Campus Benjamin Franklin, 12203 Berlin, Germany.
8. DZHK (German Centre for Cardiovascular Research), partner site Berlin, Germany.
9. Department of Sports Medicine, Charité-Universitätsmedizin Berlin, Humboldt University of Berlin, 10117 Berlin, Germany.
10. Cologne Center for Genomics (CCG), Medical Faculty, University of Cologne, Cologne, Germany.
11. Institute of Computational Biology, German Research Center for Environmental Health, Helmholtz Zentrum München, Neuherberg, Germany.
12. Department of Computer Science, TUM School of Computation, Information and Technology, Technical University of Munich, Garching, Germany.
13. Medizinische Klinik und Poliklinik I, LMU University Hospital, Munich, Germany.
14. DZHK (German Centre for Cardiovascular Research), partner site Munich Heart Alliance, Munich, Germany.
15. Klinik für Herz- und Kreislauferkrankungen, Deutsches Herzzentrum München, Technische Universität München, 80636 Munich, Germany.
16. Department of Cardiology, Pulmonology, and Vascular Medicine, Medical Faculty and University Hospital, Heinrich Heine University, Düsseldorf, Germany.
17. Cardiovascular Research Institute Düsseldorf (CARID), Heinrich Heine University, Düsseldorf, Germany.
18. Institute for Cardiovascular Regeneration, Goethe University Frankfurt, Germany.
19. Cardiopulmonary Institute, Goethe University Frankfurt am Main, Germany.

** These authors contributed equally to this work.*

© The Author(s) 2026. Published by Oxford University Press on behalf of the European Society of Cardiology. This is an Open Access article distributed under the terms of the Creative Commons Attribution-NonCommercial License (https://creativecommons.org/licenses/by-nc/4.0/), which permits non-commercial re-use, distribution, and reproduction in any medium, provided the original work is properly cited. For commercial re-use, please contact reprints@oup.com for reprints and translation rights for reprints. All other permissions can be obtained through our RightsLink service via the Permissions link on the article page on our site—for further information please contact journals.permissions@oup.com.

ACCEPTED MANUSCRIPT

Downloaded from academic.oup.com/cardiovascres/advance-article/doi/10.1093/cvr/cvag258/9005686 by guest on 03 November 2026

***These authors are co-senior authors*

Correspondence:

Teresa Gerhardt, M.D.

Institute for Cardiovascular Regeneration

Goethe University Frankfurt

Theodor-Stern-Kai 7

60590 Frankfurt am Main, Germany

Email: t.gerhardt@med.uni-frankfurt.de

Graphical abstract

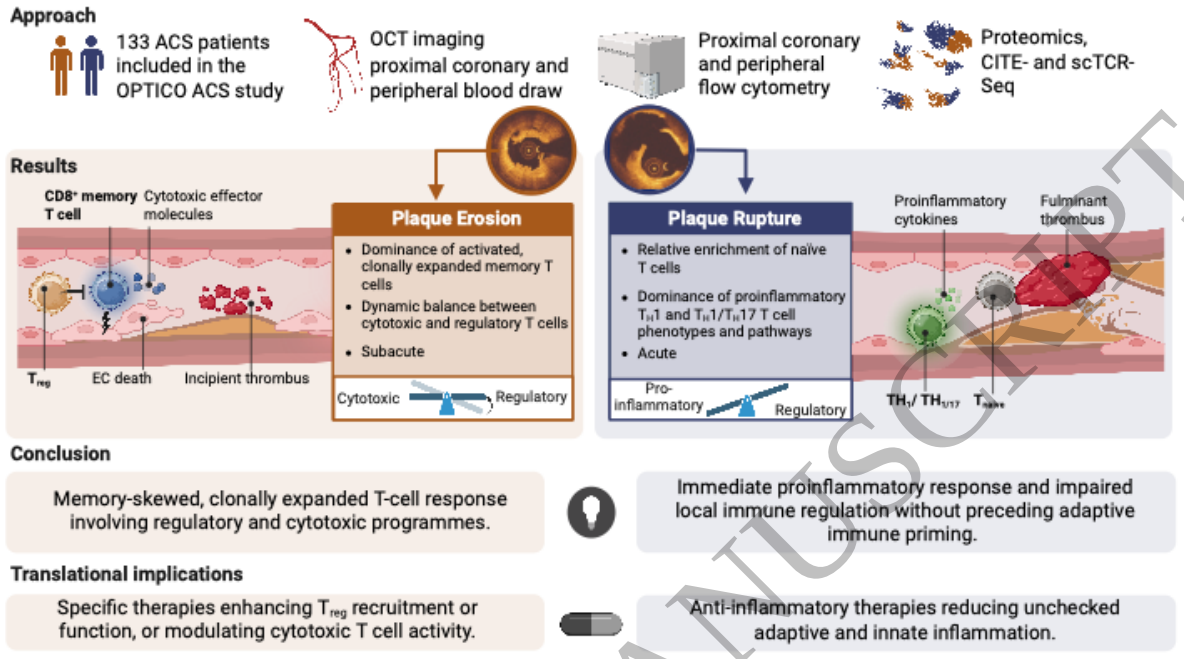
Key Question: How do local T cell composition, activation, functional programming, and clonality differ between plaque rupture and erosion in ACS?

Key Finding: Erosion and rupture are immunologically distinct. Erosion features antigen-experienced, clonally expanded regulatory and cytotoxic T cells, whereas rupture is characterized by proinflammatory phenotypes, diverse TCR repertoires, and heightened inflammatory signaling.

Take Home Message**:** Immune profiling of ACS coronary culprit-lesion blood reveals distinct local T cell signatures in plaque erosion versus rupture, suggesting divergent immunologic trajectories. These findings support precision ACS therapy: Targeting adaptive immunity in erosion and established inflammatory and innate pathways in rupture.

ACCEPTED MANUSCRIPT

Downloaded from academic.oup.com/cardiovascres/advance-article/doi/10.1093/cvr/cvag258/9005686 by guest on 03 November 2026



Graphical abstract. ACS = acute coronary syndrome; CITE-seq = Cellular Indexing of Transcriptomes and Epitopes by sequencing; EC = endothelial cell; OCT = optical coherence tomography; TCR-seq = T cell receptor sequencing; TH1 / TH1/17 = T-helper type 1 and T- helper type 1/17 cell; Treg = regulatory T cell.

Translational Perspective

Plaque erosion and plaque rupture represent biologically distinct causes of ACS, yet current treatment algorithms do not tailor therapy to the underlying mechanism. Our findings suggest that broad anti-inflammatory therapies targeting both adaptive and innate immune pathways, such as colchicine or IL-1β blockade, may be more effective in suppressing the pro-inflammatory activation associated with plaque rupture. In contrast, erosion is characterized by memory-skewed, clonally expanded regulatory and cytotoxic T cells. Strategies specifically enhancing

ACCEPTED MANUSCRIPT

Downloaded from academic.oup.com/cardiovascres/advance-article/doi/10.1093/cvr/cvag258/9005686 by guest on 03 November 2026

Treg function (e.g., low-dose IL-2) or modulating $CD8^+$ T cell cytotoxicity (e.g., granzyme inhibitors) may mitigate endothelial injury and thrombus progression in erosion. Together, these insights highlight lesion-specific immunomodulation as a promising route toward precision therapy in ACS.

Introduction

More than 7 million people worldwide suffer from acute coronary syndromes (ACS) each year(1). Despite major advances in secondary prevention, including intensified lipid-lowering beyond statins(2, 3), enhanced antithrombotic strategies(4) , and anticoagulation(5, 6, 7), the burden of recurrent cardiovascular (CV) events remains unacceptably high(8), with a 5-year recurrence rate recently reported at 33.4% following an ACS index event(9). Traditionally, ACS was considered a homogeneous condition, primarily driven by plaque rupture. Rupture is characterized by the disruption of a thin fibrous cap overlying a lipid-rich, highly inflamed coronary atherosclerotic plaque(10, 11, 12). However, high-resolution in vivo imaging using optical coherence tomography (OCT) has challenged the paradigm of homogeneity, identifying plaque erosion as a distinct mechanism underlying 30–40% of ACS cases(12, 13). In erosion, a thrombus forms atop an intact fibrous cap covering a matrix-rich, lipid- and leukocyte-poor lesion, typically associated with endothelial denudation rather than extensive structural disruption. A growing body of histopathological(14, 15), laboratory(14, 16, 17, 18, 19, 20), imaging(21, 22, 23), and clinical(18, 24, 25) evidence points towards fundamental differences in vascular inflammation and immune

ACCEPTED MANUSCRIPT

Downloaded from academic.oup.com/cardiovascres/advance-article/doi/10.1093/cvr/cvag258/9005686 by guest on 03 November 2026

responses between erosion- and rupture-driven ACS. This has raised the possibility that tailored therapeutic strategies based on culprit lesion pathophysiology could address residual inflammatory risk in ACS(18). However, the cellular and molecular mechanisms underlying plaque erosion, particularly those required to guide precision immunomodulatory therapies, remain poorly understood.

Distinct accumulation patterns of immune cells, particularly $CD4^+$ and $CD8^+$ T cells, have been described in plaque rupture and plaque erosion. In flow cytometry of peripheral venous blood, patients with non-ST elevation myocardial infarction (NSTEMI-ACS) caused by plaque rupture showed skewed $CD4^+$ T cell differentiation towards higher levels of long-lived $CD4^+CD28_{null}$ T cells, compared to those with plaque erosion(19). Comparative flow cytometric analyses of local and systemic leukocyte profiles in erosion-associated ACS have revealed selective enrichment of adaptive immune cells, particularly $CD4^+$ and $CD8^+$ T cells and their effector molecules, within the proximal coronary microenvironment(14, 23, 26). While this supports a differential role of T cells in erosion versus rupture, their phenotypic diversity and functional states remain poorly defined. Given the profound heterogeneity of T cells in ACS, including diverse cellular differentiation stages, effector functions, antigen specificities, and context-dependent inflammatory or reparative activity(27, 28), mere enumeration of $CD4^+$ and $CD8^+$ T cells is insufficient. Here, we integrate clinical and imaging data with flow cytometry, plasma proteomics, single-cell indexing of transcriptomes and epitopes by sequencing (CITE-seq), and paired T cell receptor sequencing to comprehensively characterize the phenotypic differentiation states, transcriptional programs, and clonal architecture of T cells in the proximal culprit-lesion microenvironment of plaque erosion and rupture. Through this multi-omic profiling of intracoronary blood, we delineate the distinct T cell immune profiles that accompany erosion and rupture, addressing a key knowledge gap in the immunobiology of ACS.

ACCEPTED MANUSCRIPT

Downloaded from academic.oup.com/cardiovascres/advance-article/doi/10.1093/cvr/cvag258/9005686 by guest on 03 November 2026

Methods

Data availability. All transcriptomics data used in this study will be made publicly available in the Gene Expression Omnibus (GEO) under accession number GSE344379.

Code availability. *In silico* analysis was performed using custom R scripts based on the recommended pipelines from pre-existing packages listed below. No new algorithms central to the findings of this manuscript were developed. Custom R scripts are available in a GitHub-Repository (https://github.com/haukeh90/Multiomics_OPTICO_ACS_Study).

Study design and patients. The current study represents a sub-study of the translational OPTIcal-COherence Tomography in Acute Coronary Syndrome (OPTICO-ACS)-study program(14, 18, 20, 23). The study program was a prospective, multicentric trial coordinated by Charité – University Medicine Berlin and the Berlin Institute of Health (BIH), Germany. Its primary endpoint was to evaluate prognostic differences between plaque erosion and plaque rupture(18). Secondary endpoints included clinical- and OCT-based patient characterization(23) and detailed immunophenotyping of both groups(14, 18, 20). For this sub-study, 133 consecutive patients presenting between April 2020 and April 2022 with NSTE-ACS(29) and STE-ACS(30) at Charité - University Medicine Berlin, Campus Benjamin Franklin, Berlin, Germany were considered. Exclusion criteria included any acute or chronic infections, including COVID-19, and inflammatory conditions, as well as therapy with immunomodulatory or anti-inflammatory agents. Upon enrolment, eligible patients underwent coronary angiography, followed by OCT imaging of the ACS-causing culprit lesion. Further details, including a full list of clinical and angiographic exclusion criteria, were recently published(14, 18, 20). All OCTs were analyzed for the underlying ACS-causing culprit pathophysiology by two independent core labs (Charité University Medicine,

ACCEPTED MANUSCRIPT

Downloaded from academic.oup.com/cardiovascres/advance-article/doi/10.1093/cvr/cvag258/9005686 by guest on 03 November 2026

Berlin, and German Heart Centre, Munich, Germany) using Medis QIvus 3.0 (Medis Medical Imaging Service, Leiden, Netherlands), according to the predefined study-specific standard operating procedure(14) and as previously reported(14, 25). The OPTICO-ACS trial was registered at ClinicalTrials.gov (NCT03129503) and conducted in accordance with the Declaration of Helsinki. Written informed consent was obtained from all participating patients. The local ethics committee at Charité University Berlin provided ethical approval (No. EA1/270/16).

Collection and storage of biomaterial. Blood collection and processing methods in the OPTICO-ACS study have been previously described(14). After diagnostic angiography and before OCT imaging and percutaneous coronary intervention (PCI), peripheral blood samples were obtained by aspiration of 30 ml blood from the arterial sheath in the distal radial artery as an individual systemic baseline for inflammatory characterization. Coronary arterial blood samples were obtained during cardiac catheterization by positioning the Export Advance™ aspiration catheter system (Medtronic, Minneapolis, MN, USA) directly into the proximal culprit-vessel segment adjacent to the occlusive thrombotic lesion with subsequent aspiration of 30 ml blood. Ethylenediaminetetraacetic acid (EDTA)-supplemented samples were filtered through a 40 µm cell strainer within a maximum of 60 minutes after withdrawal. Whole blood was analyzed by flow cytometry (for overall cell counts, including granulocytes) and peripheral blood mononuclear cells (PBMCs) were isolated by continuous density gradient centrifugation. For this, blood was diluted 5:4 with phosphate-buffered saline (PBS) containing 2 mM EDTA and carefully layered on Ficoll-Paque (ratio 2:1). Samples were centrifuged for 30 min, 500 x g, at 20°C. PBMCs were collected on the surface of the Ficoll layer, washed twice in PBS at room temperature, and resuspended at $1x10^6$ PBMCs/ml in freezing medium (Roswell Park Memorial Institute (RPMI) 1640 supplemented with 10% fetal bovine serum (FBS) and 10% dimethyl sulfoxide (DMSO)). Aliquots

ACCEPTED MANUSCRIPT

Downloaded from academic.oup.com/cardiovascres/advance-article/doi/10.1093/cvr/cvag258/9005686 by guest on 03 November 2026

were gradually cooled in Mr. Frosty freezing containers over 24 hours and transferred into liquid nitrogen until further analysis.

Flow cytometry. Peripheral and coronary blood samples (3x 100 µl) were stained with three different cocktails of fluorochrome-labelled antibodies, followed by a 1:10 dilution/fixation in 0.5% phosphate-buffered paraformaldehyde solution. Whole blood was used for broad cell enumeration including granulocytes; PBMCs were used for T cell phenotyping. Samples were acquired 16–24 hours post-fixation on an Attune NxT Acoustic Focusing Flow Cytometer (Thermo Fisher Scientific, Waltham, MA, USA) and data were analyzed with Kaluza v1.5 (Beckman Coulter, Brea, CA, USA). For stimulation-based intracellular cytokine and validation assays, PBMCs were rested overnight in RPMI 1640 media (Thermo Fisher, Cat# 21875034) supplemented with 10% FCS (Merck, Cat# F3018), 1% nonessential amino acids (Thermo Fisher, Cat# 11140050), 25 mM HEPES (Thermo Fisher, Cat# 15630056), 1 mM sodium pyruvate (Thermo Fisher, Cat# 11360070), and 1% penicillin/streptomycin (Thermo Fisher, Cat# 10378016). Cells were stimulated with PMA/ionomycin (eBioscience stimulation cocktail; Thermo Fisher, Cat# 00-4970-03) for 2 hours, followed by addition of GolgiPlug (BD Biosciences, Cat# 555029) to inhibit protein transport for additional 2 hours. Following stimulation, cells were incubated with human Fc block (BioLegend, Cat# 422302), anti-human CD45RA, and LIVE/DEAD Blue (Thermo Fisher, Cat# L23105) to exclude dead cells, then stained for chemokine receptors and surface markers in brilliant staining buffer (Thermo Fisher, Cat# 00-4409-42) diluted in FACS buffer (PBS, 2% FCS). For intracellular cytokine staining, cells were fixed and permeabilized using the Cytofix/Cytoperm kit (BD Biosciences, Cat# 554714) per the manufacturer's instructions and stained in perm buffer (BD Biosciences, Cat# 554723). Cells were acquired on a five-laser-equipped Aurora flow cytometer (Cytek Biosciences). To determine the culprit ratio, the proportion of each indicated population in coronary blood was normalized to its equivalent measured systemically at the

ACCEPTED MANUSCRIPT

Downloaded from academic.oup.com/cardiovascres/advance-article/doi/10.1093/cvr/cvag258/9005686 by guest on 03 November 2026

arterial sheath. All analyses were performed by a researcher blinded to all OCT diagnoses. Flow cytometry data were analyzed with Flowjo (v.10.10.1 Water Biosciences)

Proteomics. Multiplex plasma proteomic analyses were performed on coronary arterial plasma samples of patients with plaque erosion and rupture obtained during the index procedure. After matching for age, sex, and cardiovascular risk factors, samples were assessed for 384 inflammation-associated proteins (Olink Explore 384 Inflammation panel) using Olink® Proximity Extension Assay (PEA) technology as previously described(18).

CITE-seq. CITE-seq was performed on matched patients with plaque rupture (n=8) and erosion (n=8). The CITE-seq workflow was performed based on a published protocol(31) at the Cologne Center for Genomics (CCG). All experiments were performed in low protein-binding plasticware. For profiling of cell surface proteins, the commercial 137-target TotalSeq™-C Human Universal Cocktail V1.0 (BioLegend Cat. No. 399905), containing antibody-derived tags (ADTs) for 130 different cell surface antigens and 7 isotype controls, was used. 3 Hashtag antibodies (TotalSeq™-C 0251 anti-human Hashtag 1 (Barcode Sequence GTCAACTCTTTAGCG); TotalSeq™-C 0252 anti-human Hashtag 2 (Barcode Sequence TGATGGCCTATTGGG); TotalSeq™-C 0253 anti-human Hashtag 3 (Barcode Sequence TTCCGCCTCTCTTTG), all clone LNH-94; 2M2) were used for multiplexing. Lyophilized antibody-derived tags (ADT)-reagents and -hashtags were reconstituted and mastermixes prepared according to the manufacturer's instructions. To minimize batch effects, all 16 samples were divided into two groups of 8 samples, each with 4 plaque erosions and 4 plaque ruptures. Samples were processed on two consecutive days, 8 per day respectively. PBMCs were thawed by agitation in a 37°C water bath. Samples were washed three times using pre-warmed (37°C) Cell Staining Buffer (BioLegend, Cat. No

ACCEPTED MANUSCRIPT

Downloaded from academic.oup.com/cardiovascres/advance-article/doi/10.1093/cvr/cvag258/9005686 by guest on 03 November 2026

420201), counted and assessed for viability by trypan blue staining. In case of a viability <85%, the patient sample was removed and replaced with another sample from the same patient to ensure high sample- and data quality. Cells were incubated with FcX block (BioLegend, Cat. No 422302) for 10 min, followed by incubation with a mastermix containing the ADT-panel and one hashtag for 30 min at 4°C, washed three times, and filtered through a 40 µm cell strainer. Cells were stained for viability using Propidium Iodide (Thermo Fisher, Cat. No P1304MP), and 50.000 viable cells per sample were sorted with a FACSAria Fusion cell sorter (BD Biosciences, Franklin Lakes, NJ, USA). Samples were pooled in equal proportions, and 43.000 cells were loaded per lane of a 10x Genomics Chip K. CITE-seq and paired TCR profiling was performed using the Chromium Next GEM Single Cell 5′ Kit v2 (PN-1000263). Libraries were prepared using the Library Construction Kit (16 rxns, PN-1000190), the 5′ Feature Barcode Kit (PN-1000541), and the Chromium Single Cell Human TCR Amplification Kit (PN-1000252). Dual indexing was performed with the Dual Index Kit TT Set A (PN-1000215) and Dual Index Kit TN Set A (PN-1000250). Library preparation included 11 cycles for cDNA synthesis, followed by: (1) 14 cycles for gene expression libraries, (2) 8 cycles for CITE-seq libraries, and (3) TCR enrichment performed in two rounds (12 and 10 cycles), followed by an additional 8 cycles for TCR library preparation. All libraries were sequenced on a NovaSeq 6000 (Illumina) at the CCG core. Gene expression libraries were sequenced at a depth of 25,000 reads per cell (~750 million reads per reaction), while CITE-seq and TCR libraries were sequenced at 5,000 reads per cell (~150 million reads per multiplexed reaction)

Single-cell RNA and ADT data processing. Sequencing data were converted from BCL to FASTQ format using Illumina's *bcl2fastq*. Cell Ranger Multi v6.1.2 (10x Genomics Cloud Analysis) was used for alignment and quantification of gene expression, ADTs, and V(D)J repertoire, using the GRCh38 v5.0.0 reference genome. Raw count matrices for RNA and ADT expression were

ACCEPTED MANUSCRIPT

Downloaded from academic.oup.com/cardiovascres/advance-article/doi/10.1093/cvr/cvag258/9005686 by guest on 03 November 2026

imported as individual Seurat objects. **Doublets were identified and removed using DoubletFinder(32), and cells were filtered using the following QC thresholds: nFeature_RNA > 500, nFeature_RNA < 4000 and percent.mt < 8.** After quality control, RNA and ADT data were processed first separately and then analysed jointly with Weighted-nearest neighbor (WNN) integration:

- **Pre-processing and integration of RNA data:** Raw RNA counts were normalized using the *NormalizeData* function in Seurat (v5.0.1), and 2,500 variable features were identified using variance-stabilizing transformation (vst). After identification of variable features, datasets were scaled and subjected to principal component analysis (PCA) using the selected features. Anchors were identified using reciprocal PCA (RPCA) with *FindIntegrationAnchors*, and datasets were integrated using *IntegrateData* (dims = 1:30, k.anchor = 20). Per-patient QC metrics are provided in **DataFileS1**.
- **Pre-processing and integration of ADT data:** ADT counts were normalized using denoised and scaled by background (DSB) normalization(33). Integration features were selected across pools, PCA was performed on each object using all ADT features, and anchors were identified via RPCA. ADT data were then integrated using *IntegrateData* and dims = 1:30.

Transcriptional similarity analysis. To assess whether culprit-proximal coronary immune cells transcriptionally resemble atherosclerotic plaque or circulating blood, OPTICO-ACS profiles were compared against six independent scRNA-seq reference cohorts (n = 151 donors): coronary plaque(34), carotid plaque(35, 36, 37), healthy and STEMI peripheral blood(38), and peripheral blood from ACS patients with OCT-defined erosion or rupture(39). All datasets were processed through an identical pipeline (normalization, variance-stabilizing selection of 2,000 variable genes, uniform QC: nFeature_RNA 500–4,000, nCount_RNA < 17,500, percent.mt < 8), with non-

ACCEPTED MANUSCRIPT

Downloaded from academic.oup.com/cardiovascres/advance-article/doi/10.1093/cvr/cvag258/9005686 by guest on 03 November 2026

immune cells removed from the coronary plaque references and low-quality donors (<200 cells, low complexity, or high haemoglobin content) excluded. For each donor, a pseudobulk profile was generated by aggregating log-normalized expression across shared variable genes (AggregateExpression), and pairwise similarity was quantified as the Spearman correlation between donors, visualized by unsupervised hierarchical clustering. A plaque similarity index was defined per donor as the mean Spearman correlation to a combined plaque reference (carotid + coronary), and compared between Erosion and Rupture by Wilcoxon rank-sum test.

ACCEPTED MANUSCRIPT

Downloaded from academic.oup.com/cardiovascres/advance-article/doi/10.1093/cvr/cvag258/9005686 by guest on 03 November 2026

Non-negative Matrix Factorization (NMF) and metaprogram discovery. To uncover latent gene expression programs, non-negative matrix factorization (NMF) was performed using the GeneNMF package(40, 41, 42). The RNA assay was used as input, and the Seurat object was split by patient identifier to retain biological variability. For each patient-specific dataset, the top 2,000 variable genes were selected, and gene expression matrices were centered before factorization. This unsupervised, annotation-independent approach captures continuously varying and cross-cutting transcriptional programs that cluster-based differential expression alone cannot resolve. Because TCR genes reflect clonal identity and expansion rather than functional cell state and can confound phenotypic interpretation with clonotype-level signals, all TCR V/J/C/D genes were excluded from the feature space prior to highly variable gene selection and NMF decomposition. The *multiNMF* function was used to perform NMF across a range of factorization ranks (k = 4 to 9) with L1 regularization set to zero. Six robust metaprograms were extracted using *getMetaPrograms*, which computes consensus metaprograms by hierarchical clustering (method: "ward.D2") and filters genes with a confidence score ≥ 0.25. Similarity between metaprograms was visualized by Jaccard distance and plotted as a heatmap. The metaprogram gene sets were used to calculate single-cell module scores using UCell. Scores were computed for each cell using a Mann-Whitney U-statistic and are mathematically related to the AUC (area under the ROC curve). Module scores were added to the Seurat object and visualized using dot plots. To assign biological meaning to each metaprogram, gene set enrichment analysis was conducted using fgsea and MSigDB gene sets(43). Both KEGG (C2:KEGG) and Gene Ontology Biological Processes (C5:BP) categories were queried using the top-ranked genes of each metaprogram. Metaprogram scores were used to rank cells by disease condition (rupture vs. erosion).

ACCEPTED MANUSCRIPT

Downloaded from academic.oup.com/cardiovascres/advance-article/doi/10.1093/cvr/cvag258/9005686 by guest on 03 November 2026

WNN integration

Integrated RNA and ADT PCA reductions were merged into a single Seurat object. Multimodal neighbors were computed using *FindMultiModalNeighbors*, combining the top 30 RNA and top 18 ADT principal components. WNN-based Uniform Manifold Approximation and Projection (UMAP) was performed with parameters a = 0.8, b = 0.8 to control minimum distance and spread. Clustering was conducted using the weighted shared nearest neighbor (wsnn) graph and the SLM algorithm (resolution = 0.5).

Cluster annotation

WNN-based clusters were annotated based on canonical marker gene and surface protein expression, aided by reference-mapping to an established CITE-seq PBMC atlas using Azimuth(44). Clusters were subsequently grouped in two resolutions:

- **Res1:** Major immune cell types (e.g., Mono, $CD4^+$, $CD8^+$, B, NK, DC)
- **Res2:** Fine-grained subsets (e.g., $CD14^+$ Mono, $CD4^+$ T_{CM} T_{EM}, cDC, Plasmablast)

Differential gene expression analysis

Cluster-specific DE genes/proteins were identified between clusters of cells using the *FindAllMarkers* function for both RNA and ADT assays. For each resolution, cell-specific markers were computed using a Wilcoxon rank-sum test (min.pct = 0.25, logfc.threshold = 0.25, only.pos = TRUE) with **p-values adjusted by Bonferroni correction**, and the top 10 markers per cluster were visualized using heatmaps.

ACCEPTED MANUSCRIPT

Downloaded from academic.oup.com/cardiovascres/advance-article/doi/10.1093/cvr/cvag258/9005686 by guest on 03 November 2026

Pseudobulk differential gene expression

To account for patient-level variation, differential gene expression between patients with Rupture and Erosion was performed using pseudobulk analysis applying the edgeR algorithm within the Libra framework(45, 46). Gene counts were aggregated per patient and cluster and group comparisons were conducted between erosion and rupture samples using likelihood ratio testing (LRT).

Pathway analysis

Pathway enrichment analysis was conducted using the express analysis function of Metascape(47). All TCR V/J/C/D genes were excluded to avoid potential confounding of phenotypic interpretation. Pathways with an adjusted p-value < 0.05 after Bonferroni correction were considered statistically significant. Selected pathways were visualized using bar plots (based on p-values) or spider plots.

T cell subclustering

$CD4^+$ and $CD8^+$ T cells were subclustered using ADT expression data from the integrated Seurat object. A panel of 33 T cell-relevant ADT markers (e.g., CD3, CD4, CD8, CD25, PD-1, CTLA-4, CD127, CD39) was selected as variable features. The dataset was scaled using these features prior to downstream analysis.
To account for batch effects, the dataset was split and singular value decomposition (SVD) was conducted, and reciprocal LSI (rLSI)–based integration was performed using the *FindIntegrationAnchors* and *IntegrateData* functions (dims = 1:15). SVD-based UMAP was performed with parameters a = 0.8, b = 0.8 to control stretch and density. Clustering was

ACCEPTED MANUSCRIPT

Downloaded from academic.oup.com/cardiovascres/advance-article/doi/10.1093/cvr/cvag258/9005686 by guest on 03 November 2026

performed using the Leiden algorithm (resolution = 0.6) on the integrated SVD reduction. Clusters were annotated based on canonical ADTs and cluster-specific expression patterns derived from both ADT and RNA data.

TCR analysis

Raw TCR sequencing contigs were combined across samples using the *combineTCR()* function from the scRepertoire package (v2.0.7), specifying the sample IDs and retaining all annotated clonotypes. To assess repertoire redundancy and diversity, amino acid (CTaa) and gene (Ctgene) clonotypes were extracted per sample, counted, and merged across all samples. TCR metadata was integrated into the Seurat object using the *combineExpression()* function, annotating each cell with its clonal frequency and size. Clonal expansion was visualized using UMAP projections, and clonal occupancy across annotated clusters and disease groups was analysed using *clonalOccupy()* and exported for further visualization. Clonal diversity was estimated by calculating the Chao1 indices, analyzing the full repertoire (both TRA and TRB) as well as individual chains separately. To assess whether expanded OPTICO clonotypes overlapped with published cardiovascular disease (CVD)-associated T-cell receptors, CDR3β amino-acid sequences were mapped against the curated CVD-TCR database, which compiles 2,454 disease-associated TCR sequences across six cardiovascular pathology categories from 34 independent studies. Only expanded clonotypes (clone size > 1) were retained, and TRBV gene names were harmonized to IMGT nomenclature in both datasets before comparison. Repertoire-level overlap between OPTICO groups (Erosion, Rupture) and each CVD category was quantified as the Jaccard index of shared unique CDR3β sequences. To account for clonal expansion at the single-patient level, a frequency-weighted overlap score was computed per patient as the summed cell frequency of CDR3β sequences shared with a given CVD category, divided by that patient's total cell count, and compared between Erosion and Rupture using unpaired Wilcoxon rank-sum tests.

ACCEPTED MANUSCRIPT

Downloaded from academic.oup.com/cardiovascres/advance-article/doi/10.1093/cvr/cvag258/9005686 by guest on 03 November 2026

Public CDR3β sequences shared between OPTICO and the database were additionally visualized as binary presence heatmaps.

Statistical analysis

The Shapiro-Wilk test was performed to assess the Gaussian distribution of data, assisted by graphical evaluation of the distribution. Chi^2 tests were performed when comparing categorical variables. Fisher's exact test was applied instead when expected counts were less than five. Mann-Whitney U-tests were used for two-group comparisons of continuously distributed variables in the absence of a Gaussian distribution; otherwise, independent t-tests were performed. Odds ratios (ORs) comparing the frequency of cell clusters between rupture and erosion were calculated by constructing 2x2 contingency tables per cluster (presence vs. absence in rupture vs. erosion), followed by OR estimation using Fisher's exact test. All used tests were two-sided; $p<0.05$ was considered statistically significant. The statistical tests applied in the CITE-seq analysis are detailed above.

ACCEPTED MANUSCRIPT

Downloaded from academic.oup.com/cardiovascres/advance-article/doi/10.1093/cvr/cvag258/9005686 by guest on 03 November 2026

Results

Enrolment and baseline characteristics

This sub-study of the OPTICO-ACS trial included 133 patients presenting with NSTEMI-ACS or STEMI-ACS. After clinical and technical screening, 93 patients underwent successful OCT imaging with sufficient quality for plaque morphology assessment and were eligible for further immunophenotyping. Of these, 77 had flow cytometry data of sufficient quality and were categorized according to underlying ACS pathology: 49 (64%) with plaque rupture, 21 (27%) with plaque erosion, and 7 (9%) with other causes such as spontaneous coronary artery dissection or calcified nodules, which were excluded from further analysis (**Figure 1**). Baseline characteristics of patients with plaque rupture and erosion are provided in **Supplementary Material 1**. No significant differences were observed in age ($p = 0.64$), sex ($p = 1.00$), or typical cardiovascular risk factors. Patients with plaque rupture exhibited significantly higher total cholesterol and LDL cholesterol levels. Rupture and erosion patients were equally likely to present with STE-ACS ($p = 0.23$). A subset of 16 patients (8 with rupture, 8 with erosion) matched by age, sex, and cardiovascular risk profile was selected for high-resolution immune profiling using CITE-seq and TCR-seq (**Supplementary Material 2**, **DataFileS1**).

Paired culprit-proximal immunophenotyping reveals divergent T-cell and proteomic signatures in plaque erosion and rupture

The intracoronary aspirate was collected from the culprit artery before balloon inflation and stenting, using an aspiration catheter positioned proximal to the thrombus (**Figure 2a**). To identify culprit-site immune enrichment relative to each patient's systemic background, we calculated a coronary-to-peripheral "culprit ratio" (CR): the intracoronary measurement divided by the paired peripheral arterial measurement obtained at the same time (**Figure 2a**). Lineage profiling by flow

ACCEPTED MANUSCRIPT

Downloaded from academic.oup.com/cardiovascres/advance-article/doi/10.1093/cvr/cvag258/9005686 by guest on 03 November 2026

cytometry of paired peripheral and proximal coronary blood samples (**Figure 2a** and **Supplementary Material 3-10)** showed distinct immunophenotypic signatures between patients with ACS caused by plaque erosion or rupture. Confirming previous findings(14), plaque erosion patients exhibited significantly elevated CRs for $CD4^+$ T cells, $CD8^+$ T cells, and B cells (**Supplementary Material 5a**). CRs of monocytes and granulocytes were not different between groups. The proportion of these immune subsets was unchanged when directly comparing proximal coronary or peripheral compartments separately across culprit lesion phenotypes (**Supplementary Material 5b and c**).

Given this pronounced difference in the distribution of adaptive immune cells in plaque erosion, we next asked whether this accumulation reflected differences in T cell differentiation state (**Supplementary Material 6**). **T cell differentiation status was defined using a gating hierarchy distinguishing naïve,** terminally differentiated effector memory (TEMRA)**, central memory (TCM), and effector memory (TEM) populations (Figure 2b, Supplementary Material 6).** Patients with plaque erosion exhibited significantly higher proportions of proximal memory $CD4^+$ and $CD8^+$ T cells, as well as markedly higher CRs in both compartments, compared to patients with plaque rupture **(Figure 2c).** By contrast, rupture showed a relative shift toward a less differentiated T cell phenotype, with higher proportions and CRs of $CD4^+$ and $CD8^+$ naïve-phenotype T cells compared with erosion **(Supplementary Material 7&8)**, suggesting fundamentally divergent patterns of T cell accumulation and differentiation between erosion and rupture.

These differences in T cell differentiation prompted us to further investigate their functional polarization (**Supplementary Material 9)**. T cells from plaque erosion were skewed toward anti-inflammatory regulatory T cells (T_{regs}) (**Figure 2d**). Interestingly, in contrast to the proximal coronary data, peripheral T_{regs} were more abundant in patients with plaque rupture (**Supplementary Material 10**). Culprit-proximal non-naïve T cells in plaque rupture exhibited a

ACCEPTED MANUSCRIPT

Downloaded from academic.oup.com/cardiovascres/advance-article/doi/10.1093/cvr/cvag258/9005686 by guest on 03 November 2026

predominance of pro-inflammatory CD4+ T cell subsets, with significant coronary accumulation of T-helper type 1 (T_H1) cells and T-helper type 1–type 17 (T_H1/T_H17) cells (**Figure 2d**) – a pattern also partially reflected peripherally, with elevated circulating T_H1/T_H17 cells (**Supplementary Material 10**). To account for the compositional nature of CD4+ T-helper frequencies, we complemented frequency-based analyses with proximal coronary cell count comparisons (**Supplementary Material 11**) and applied a centered log-ratio (CLR) transformation. Frequency- and count-based comparisons were directionally concordant across subsets. CLR analysis confirmed T_{reg} enrichment in erosion and T_H1/T_H17 enrichment in rupture, indicating that these differences were not solely attributable to compositional constraints. In contrast, T_H1 differences were no longer significant, suggesting that the apparent frequency shift in T_H1 cells may largely reflect reciprocal changes in other subsets.

These opposing immunologic profiles were reflected in elevated CRs for T_{regs} in erosion and for T_H1 and T_H1/T_H17 cells in rupture (**Figure 2e**). No significant differences were observed in other lesional T_H-subsets, peripheral T-helper cell profiles, or CRs between plaque erosion and plaque rupture (**Figure 2d, e**). Overall, the proximal coronary microenvironment of ACS caused by plaque erosion was associated with enhanced accumulation of regulatory T cells, whereas plaque rupture was characterized by a less differentiated T-cell profile overall, with a relative enrichment of proinflammatory effector phenotypes among functionally polarized CD4+ T cell subsets (**Figure 2e).**

To assess whether the distinct cellular profiles observed by flow cytometry were associated with corresponding differences in local immune signaling, we performed targeted inflammatory multiplex proteomics from culprit lesion plasma (**Figure 2f**). Consistent with the local enrichment of T_{reg} and memory CD4+ T cells, erosion samples had higher levels of proteins involved in T cell activation, immune regulation, and T_{reg} polarization, including interleukin (IL)-2, CD6, CD58, and protein kinase C theta (PRKCQ), proteins known to support T cell co-stimulation and signaling(48,

ACCEPTED MANUSCRIPT

Downloaded from academic.oup.com/cardiovascres/advance-article/doi/10.1093/cvr/cvag258/9005686 by guest on 03 November 2026

49, 50). Transforming growth factor beta 1 (TGF-β1) and IL-16, which are associated with immune modulation and tissue repair(51, 52), were also elevated. Notably, increased expression of MHC class I-related chain B and A (MICB and MICA), which are stress ligands that activate cytotoxic lymphocytes through the NKG2D receptor(53), was also observed, in line with the local accumulation of $CD8^+$ effector T cells in erosion samples. In contrast, coronary aspirates from patients with ruptured lesions showed elevated levels of proteins associated with proinflammatory and innate immune signaling. These included tumor necrosis factor alpha (TNF-α), IL-17F, and C-C motif chemokine ligand 3 (CCL3), as well as IL-1 receptor antagonist (IL-1Ra), SH2 domain-containing protein 1A (SH2D1A), complement component 1q subunit A (C1qA), and MER tyrosine-protein kinase (MERTK). Together, these proteins are involved in cytokine signaling, complement activation, and phagocytic clearance mechanisms, consistent with heightened inflammatory and innate immune activity in rupture(54, 55).

Single-cell multi-omics uncovers distinct T cell activation and functional programs in erosion and rupture ACS

To further dissect the functional and molecular phenotypes underlying these divergent site-specific immune responses observed by flow cytometry, we performed single-cell multi-omic analyses. Given the limited resolution of transcriptomic data alone in distinguishing phenotypically and functionally distinct T cell subsets(36, 56, 57, 58, 59), and to capture both cellular states and clonal T cell dynamics, we employed CITE-seq(31) coupled with TCR profiling on culprit-proximal PBMCs from 8 erosion and 8 rupture patients matched for age, sex, and cardiovascular risk factors, yielding 96,391 cells after quality control.

Because blood sampled proximal to the culprit lesion may contain a mixture of circulating immune cells and lesion-associated immune signatures, we first sought to define the biological

ACCEPTED MANUSCRIPT

Downloaded from academic.oup.com/cardiovascres/advance-article/doi/10.1093/cvr/cvag258/9005686 by guest on 03 November 2026

compartment these intracoronary aspirates most closely resemble. We calculated a plaque similarity index based on the mean pseudobulk Spearman correlation between our intracoronary samples and six independent scRNA-seq reference cohorts spanning coronary plaques(34), carotid plaques(35, 36, 37), healthy peripheral blood, STE-ACS peripheral blood(38), and peripheral blood from patients with OCT-defined plaque rupture or erosion(39) (n=151 donors total) (**Figure 3a, Supplementary Material 12**). Healthy controls and peripheral STE-ACS blood showed the lowest plaque similarity (0.65), whereas culprit aspirates from both rupture and erosion patients were markedly more plaque-like (0.73–0.75), comparable to carotid and coronary plaque reference cohorts and higher than peripheral blood from ACS patients. These findings suggest that culprit aspirate immune cells are transcriptionally closer to plaque-associated immune cells than to circulating blood, consistent with a local, lesion-associated immune compartment.

To define the dominant transcriptional programs associated with the culprit-proximal immune landscape following ACS, we applied GeneNMF(40), an unsupervised matrix factorization approach, to the single-cell transcriptomes from all patients. This revealed six recurrent gene expression programs (MP1–MP6) shared across immune cell types and samples (**Figure 3b, Supplementary Material 13 and DataFileS2**), corresponding to humoral priming and antigen presentation (MP1), innate cytotoxicity (MP2), T cell memory (MP3), myeloid regulation (MP4), inflammatory amplification (MP5), and cytotoxic effector function (MP6). Program-usage analysis revealed significantly higher MP3 and MP6 activity in plaque erosion compared with plaque rupture (**Figure 3c and Supplementary Material 13**). MP3 (*memory T cell nexus*) was defined by memory-associated T cell genes, including LEF1, TCF7, CCR7, IL7R, CD27, and CAMK4, whereas MP6 was marked by cytotoxic effector genes including CD8A, GZMK, CD8B, GZMB, and ZNF683 (*cytotoxic T cell nexus*). This indicates a stronger culprit-proximal engagement of memory-associated and effector immune responses in erosion.

ACCEPTED MANUSCRIPT

Downloaded from academic.oup.com/cardiovascres/advance-article/doi/10.1093/cvr/cvag258/9005686 by guest on 03 November 2026

To contextualize these gene programs within cellular lineages, we constructed a WNN projection integrating transcriptomic and surface protein modalities, resulting in clearly defined clusters of major immune cell types *(***Figure 3d, Supplementary Material 14-16)** without any apparent batch effect between groups (**Figure 3e, f, DataFileS3-S6**). We then mapped the six metaprograms (MP1–MP6) onto this projection (**Supplementary Material 17**). The two differentially enriched programs, MP3 and MP6, localized specifically to $CD4^+$ (MP3) and $CD8^+$ (MP6) memory T cell populations, mirroring our flow cytometry findings of increased coronary accumulation of memory $CD4^+$ and $CD8^+$ T cells in erosion compared to rupture.

To determine whether the observed transcriptional differences were accompanied by shifts in immune cell composition, we compared the relative abundance of immune cell populations in erosion vs. rupture (**Supplementary Material 18**). $CD14^+$ monocytes dominated both lesion types but were similarly abundant. In contrast, T-cell composition distinguished erosion from rupture: erosion was enriched in memory $CD4^+$ and $CD8^+$ T cells, whereas rupture showed a pronounced naïve $CD4^+$/$CD8^+$ T cell bias consistent with our flow cytometry findings. Benchmarking against healthy peripheral blood reinforced this pattern, with erosion enriched in memory $CD8^+$ T cells and rupture showing more marked depletion of memory $CD4^+$ T cells (**Supplementary Material 19**). Together, these data define erosion as memory-skewed and rupture as naïve-skewed.

As the most pronounced differences were observed within the T cell compartment, we defined transcriptional alterations distinguishing erosion- and rupture-associated T cell states beyond numerical shifts. Differential gene expression (DGE) analysis within $CD4^+$ and $CD8^+$ T cells showed a higher number of regulated genes in T cells in erosion than in plaque rupture (900 and 596 in erosion, vs. 351 and 182 in rupture for $CD4^+$ and $CD8^+$ T cells, **Figure 3g**). $CD4^+$ and $CD8^+$ T cells from patients with plaque rupture exhibited increased expression of inflammation-related genes such as ***IL6ST, TNFAIP2, IFNGR2, and PRKCA,*** which are implicated in cytokine signaling, leukocyte activation, and vascular inflammation. In addition, markers of naïve and less-

ACCEPTED MANUSCRIPT

Downloaded from academic.oup.com/cardiovascres/advance-article/doi/10.1093/cvr/cvag258/9005686 by guest on 03 November 2026

differentiated T cells, including ***CCR7*** **and the costimulatory receptor** ***TMIGD2*****,** were more prominently expressed in rupture-associated T cells, consistent with the less differentiated, more naïve-like transcriptional profile in our flow cytometry data. Notably, $CD8^+$ T cells from rupture patients showed increased S100A8 and S100A9 expression, genes typically associated with myeloid and neutrophil responses but also reported in activated T cells under inflammatory stress(60, 61, 62). To validate this finding at the protein level, we performed intracellular flow cytometry for S100A8 in culprit-proximal $CD8^+$ T cells from an independent ACS cohort (Erosion n=23, Rupture n=51; **Supplementary Material 20)**. PMA/Ionomycin stimulation induced S100A8 protein in $CD8^+$ T cells from both groups, which was higher in rupture than erosion, supporting S100A8 expression as a rupture-associated feature of culprit-proximal $CD8^+$ T cells (**Supplementary Material 21**).

In contrast, erosion-associated $CD4^+$ T cells were enriched for the **costimulatory/regulatory receptors** ***GITR*** **(*****TNFRSF18*****) and** ***OX40*** **(*****TNFRSF4*****)** and for **integrin/adhesion genes (*****ITGA1*****, *****ITGB1*****),** consistent with an activated, T_{reg}-skewed and tissue-adapted phenotype, whereas erosion-associated $CD8^+$ T cells upregulated the **effector-/tissue-resident-memory granzyme** ***GZMK*****, the memory-differentiation regulator** ***HNRNPLL*****, and the integrin** ***ITGA2*****.** Both subsets shared enrichment of cell-cycle and proliferation genes (***CDCA2, CDCA3, CDC45****)* in erosion, indicating enhanced T cell turnover (**Figure 3g**, **DataFileS7**). To investigate the functional implications of transcriptional divergence in the major adaptive immune cell populations, we performed pathway enrichment analysis (**Figure 3h**). In $CD4^+$ T cells, erosion-enriched pathways included lymphocyte activation, cell adhesion and migration, cell cycle, and blood vessel development. In line with earlier findings of more proinflammatory activity in plaque rupture(18), $CD4^+$ T cells showed upregulation of cytokine production and response to type II interferon, and immune effector processes. Similarly, in the $CD8^+$ T cell compartment, rupture was associated with a broad inflammatory transcriptional signature, including upregulation of inflammatory

ACCEPTED MANUSCRIPT

Downloaded from academic.oup.com/cardiovascres/advance-article/doi/10.1093/cvr/cvag258/9005686 by guest on 03 November 2026

response, antigen processing and presentation, immune effector processes, T cell activation, and response to lipid. Conversely, erosion-associated $CD8^+$ T cells were enriched for DNA replication, cell cycle transition, integrin signaling, and cell–cell adhesion.

Cytokine response profiling reveals divergent T cell states in rupture and erosion

To assess whether the CITE-seq-defined transcriptional programs corresponded to functional cytokine activity, we used huCIRA (human Cytokine Response Analysis)(63), a framework that maps scRNA-seq profiles to reference cytokine perturbation signatures (**Figure 4a**). Applied to erosion- and rupture-associated $CD4^+$ T_{EM}/T_{CM}, $CD8^+$ T_{EM}/T_{CM}, and T_{reg} populations, huCIRA inferred a rupture-skewed type 1 cytokine response in memory T cells, including IL-2 and IFN-γ, and an erosion-skewed regulatory response in T_{regs}, including IL-10 and TSLP (**Figure 4b–e**). We validated these predictions in an independent OPTICO-ACS cohort (Erosion n=23, Rupture n=51, **Supplementary Material 20**) by stimulating proximal coronary immune cells with PMA/Ionomycin and quantifying cytokine production by flow cytometry in paired unstimulated and stimulated samples (**Figure 4f–h**). Rupture-associated $CD4^+$ T_{EM}/T_{CM} cells showed stronger induction of IL-2 than erosion-associated cells (**Figure 4f**), and rupture-associated $CD8^+$ T_{EM}/T_{CM} cells showed stronger induction of IFN-γ (**Figure 4g**). In contrast, erosion-associated T_{regs} showed stronger induction of IL-10 (**Figure 4h**). Together, these data indicate that rupture and erosion are associated with distinct functional T cell states: an inflammatory type 1 effector response in rupture and an IL-10-producing regulatory program in erosion.

Enhanced clonal expansion of T cells in plaque erosion

To gain deeper insight into the distinct T cell states differentially regulated between plaque erosion and rupture, we next performed an unsupervised subclustering of all $CD4^+$ and $CD8^+$ T cells, characterizing their heterogeneity at higher resolution (**Figure 5a, DataFileS8&S9**). This analysis

ACCEPTED MANUSCRIPT

Downloaded from academic.oup.com/cardiovascres/advance-article/doi/10.1093/cvr/cvag258/9005686 by guest on 03 November 2026

resolved multiple subsets with distinct transcriptional and proteomic profiles, including naïve, T_{CM}, T_{EM}, and terminally differentiated effector memory re-expressing CD45RA (T_{EMRA}) populations, which are often linked to cytotoxic effector function(64) (**Figure 5b**). Comparative abundance analysis by calculating ORs (**Figure 5c-d**) revealed an enrichment of effector memory cells within the CD8 and CD4 compartments (OR=0.53 & OR=0.55), as well as increased frequencies of $CD8^+$ T_{CM} (OR=0.66), T_{regs} (OR=0.78) and $CD8^+$ T_{EMRA} (OR=0.8) in erosion, indicating a shift toward a more differentiated and potentially immunoregulatory T cell phenotype in erosion. $CD8^+$ and $CD4^+$ naïve T cell subsets were enriched in the rupture microenvironment (OR=3.1 & OR=2.1), suggesting a less differentiated T cell phenotype. At the same time, smaller subsets characterized by the upregulation of inflammatory pathways at the transcriptional level (**DataFileS9**), including $CD69^+$ $CD8^+$ T_{EMRA} (OR=1.3) and $CD4^+$ T_{CM} cells (OR=1.2), were overrepresented in rupture (**Figure 5d**). Trajectory analysis of $CD4^+$ T cells, using PHATE and Slingshot, identified two differentiation paths emerging from naïve-like cells: one toward T_{regs} and one toward $CD4^+$ T_{EM} cells with increasing T_H1, T_H1/ T_H17, and T_H17 module scores (**Supplementary Material 22**). Functional validation by flow cytometry further showed that erosion-associated T_{regs} had higher IL-10, IL-17, TNF, and CXCR5 expression than rupture-associated T_{regs}. Thus, erosion is marked by activated T_{regs}, whereas rupture is characterized by a selectively expanded T_H1/T_H17 inflammatory program (**Supplementary Material 22)**. Given the enrichment of naïve T cells in rupture and effector and memory subsets in erosion, suggesting differences in activation and antigen experience, we next examined whether these phenotypic patterns were accompanied by differences in **T cell receptor clonality on a single-cell level**. Binned, enriched paired TCR clonotypes were projected onto the single-cell UMAP (**Figure 5e**), showing markedly greater clonal expansion among $CD8^+$ T cells than $CD4^+$ T cells. The expanded clonotypes were almost exclusively restricted to $CD8^+$ effector and memory subsets, including $CD8^+$ T_{EMRA} clusters and $CD8^+$ T_{EM} cells, with minimal clonal overlap in naïve populations. While both erosion and rupture contained expanded clones within similar subpopulations, the relative

ACCEPTED MANUSCRIPT

Downloaded from academic.oup.com/cardiovascres/advance-article/doi/10.1093/cvr/cvag258/9005686 by guest on 03 November 2026

distribution of clone-size categories across individual T-cell subsets varied between the two conditions (**Figure 5f**).

To characterize expanded clonotypes, we compared oligoclonal and polyclonal T cells within each disease group using DEG analysis, pathway enrichment, and transcription factor (TF) activity inference (**Figure 5g–i**). Rupture-expanded $CD8^+$ clones were enriched for cytotoxic effector genes, including *GZMB, PRF1, GNLY,* and *GZMH*, together with TCR signaling and cell-killing pathways, consistent with an acutely activated cytotoxic state. In contrast, erosion-expanded $CD8^+$ clones showed higher expression of *PDCD1*, *CX3CR1*, and *ZNF683*, enrichment of lymphocyte migration and extravasation pathways, and increased activity of *BATF, STAT1, EOMES*, and *BACH2*, suggesting a chronically stimulated effector-memory phenotype.

A similar divergence was observed among expanded $CD4^+$ clones. Rupture-expanded $CD4^+$ T cells expressed cytotoxic-associated genes, including *GNLY*, *GZMB*, *NKG7*, and *KLRD1*, and were enriched for cell killing and leukocyte degranulation pathways. Erosion-expanded $CD4^+$ clones instead showed enrichment of inhibitory and regulatory markers, including *LILRB1*, *FCGR3A*, and *KLRC4*, together with a regulatory/memory-associated TF program involving *TCF7*, *BACH2*, *FOXO1*, and *NFATC2*. The co-expression of *FCGR3A* with NK-associated inhibitory receptors (*NKG7*) and granzymes partially resembles the recently described exT_{reg} phenotype in human atherosclerosis(65), although the regulatory TF profile suggests an earlier state along the Treg-instability axis.

TCR profiling reveals clonal restriction and disease-linked clonotype sharing in erosion

To define TCR repertoire structure in erosion and rupture, we next assessed inter-patient clonotype sharing, repertoire diversity, and overlap with cardiovascular disease-associated TCR sequences (**Figure 6a**). Shared TRA and TRB clonotypes were more frequent among erosion patients than among rupture patients, with limited overlap between lesion phenotypes (**Figure**

ACCEPTED MANUSCRIPT

Downloaded from academic.oup.com/cardiovascres/advance-article/doi/10.1093/cvr/cvag258/9005686 by guest on 03 November 2026

6b). Consistently, hierarchical clustering based on TCR clonal-size distributions largely separated patients by lesion phenotype (**Figure 6c**).

Repertoire diversity analysis showed higher Chao1 richness in rupture across combined TRA/TRB, TRA-only, and TRB-only repertoires (**Figure 6d**), consistent with a broader, more polyclonal T cell repertoire. In contrast, erosion showed lower repertoire diversity, indicating greater clonal restriction and expansion of dominant T cell clones. Notably, this clonal restriction was not driven by mucosal-associated invariant T (MAIT) cells, as their abundance and clonality did not differ between erosion and rupture (**Supplementary Material 23**).

To test whether these expanded erosion-associated clonotypes overlapped with known CVD-linked TCRs, we mapped OPTICO CDR3β sequences to a CVD-TCR database, comprising 2,454 disease-associated TCR sequences across six cardiovascular pathology categories from 34 studies(66) (**Figure 6e**). Of the 19 CDR3β sequences shared between OPTICO patients and the CVD-TCR database, 17 were detected exclusively in erosion patients, 1 exclusively in rupture patients, and 1 in both groups. At the repertoire level, erosion showed higher Jaccard similarity to the distinct CVD-TCR categories than rupture (**Figure 6f**). Frequency-weighted overlap, which accounts for clonal expansion, was significantly higher in erosion for ischemic cardiac damage and atherosclerosis-associated exT_{reg} signatures, but not for the broader atherosclerosis-related category (**Figure 6g**).

Together, these findings suggest that erosion is associated with a more clonally restricted T cell repertoire enriched for expanded clonotypes overlapping CVD-linked TCR signatures, supporting disease-associated clonal selection rather than nonspecific T cell accumulation.

Discussion

This sub-study of the prospective OPTICO-ACS trial provides the first lesion-proximal multi-omics view of ACS, leveraging intracoronary blood sampled directly upstream of OCT-defined plaque

ACCEPTED MANUSCRIPT

Downloaded from academic.oup.com/cardiovascres/advance-article/doi/10.1093/cvr/cvag258/9005686 by guest on 03 November 2026

erosion and rupture. Combining multiparameter flow cytometry, multiplex proteomics, and CITE-seq with single-cell TCR-seq, we confirm enhanced local accumulation of T cells within the microenvironment of plaque erosion, consistent with our group's previous observations(14). We extend these findings by delineating the phenotypic, transcriptional, and clonal architecture of the T cell response at the culprit lesion, revealing distinct patterns of differentiation, functional polarization, and clonal expansion in plaque erosion compared to rupture. We demonstrate that erosion is defined by robust local accumulation of differentiated, clonally expanded $CD4^+$ and $CD8^+$ memory T cells. $CD4^+$ T cells in erosion-associated ACS exhibit a significant bias toward an anti-inflammatory T_{reg} phenotype, which co-accumulate alongside cytotoxic effector $CD8^+$ T cells. In contrast, rupture is characterized by an enrichment of naïve $CD4^+$ and $CD8^+$ T cells and greater polyclonality, alongside a predominance of inflammatory TH1 and TH1/TH17 subsets among differentiated Moreover, DEG analysis revealed extensive transcriptional divergence between erosion- and rupture-associated immune cells, with erosion-linked $CD4^+$ and $CD8^+$ T cells showing upregulation of pathways related to lymphocyte activation, proliferation, adhesion, and tissue residency, while rupture-associated T cells exhibited enrichment of inflammatory response, cytokine signaling, and interferon-related pathways, underscoring distinct functional programming. Together, these findings support a model in which OCT-defined plaque erosion and rupture are accompanied by distinct culprit-proximal thrombo-inflammatory responses, with erosion marked by a structured, clonally expanded adaptive T-cell program and rupture by a less differentiated but more inflammatory T-cell state.

Immune cells at the culprit lesion in plaque erosion: friends or foes?

Culprit lesions caused by plaque erosion contain fewer T cells and macrophages than those caused by plaque rupture(15, 67). Consistently, they evoke lower levels of inflammatory protein-mediators(18) and more moderate coronary inflammation assessed by imaging(22). However, a growing body of evidence suggests that altered shear stress and disturbed flow dynamics in

ACCEPTED MANUSCRIPT

Downloaded from academic.oup.com/cardiovascres/advance-article/doi/10.1093/cvr/cvag258/9005686 by guest on 03 November 2026

erosion contribute to the local accumulation of a distinct set of immune cells, which may at least in part be detrimental by promoting endothelial damage and thrombosis(14, 20, 68). Specifically, in erosion, neutrophils aspirated from the culprit lesion exhibit a unique toll-like receptor 2 (TLR2)-driven activation pattern, likely triggered by elevated hyaluronic acid, leading to matrix metalloproteinase 9 (MMP9) release and endothelial injury that could promote thrombosis(17, 20). Moreover, $CD4^+$ and $CD8^+$ T cells preferentially adhere to endothelium under conditions of disturbed laminar flow(14, 68), and can cause endothelial cell damage and trigger apoptosis when co-cultured with endothelial cells in vitro(14). In line with these observations, $CD4^+$ and $CD8^+$ T cells, along with associated cytotoxic effector molecules, show local enrichment relative to the patient's own peripheral blood in culprit-proximal blood in erosion, indicating more active recruitment or retention of T cells in erosion compared to rupture(14), a finding we confirm and substantially expand in our current study.

Accumulation of clonally expanded, antigen-experienced T cells in the erosion-associated culprit-site environment

T cell differentiation and clonal expansion are typically shaped by TCR engagement, costimulatory signals, and the local cytokine milieu, which together promote expansion and functional polarization into effector or regulatory states(27). The enrichment of memory T cells and expanded TCR clonotypes in plaque erosion is therefore consistent with prior antigen experience and clonal selection, and may reflect the systemic TCR oligoclonality we recently reported in CAD(69). This points to (likely repeated or chronic) antigen exposure before the acute event, allowing a memory pool to establish. Given the short interval between clinical presentation and intracoronary sampling, these findings are unlikely to reflect de novo generation of memory T cells during the acute event itself. Rather, they are more consistent with local recruitment, retention, or reactivation of pre-existing antigen-experienced clones at the lesion-thrombus interface. The

ACCEPTED MANUSCRIPT

Downloaded from academic.oup.com/cardiovascres/advance-article/doi/10.1093/cvr/cvag258/9005686 by guest on 03 November 2026

absence of comparable differences in peripheral T cell frequencies further supports local enrichment rather than a purely systemic expansion of this response. In contrast, plaque rupture was characterized by a higher proportion of naïve-phenotype T cells and lower clonal expansion, suggesting a less differentiated local T cell repertoire at the time of sampling. Together, these findings support a model in which plaque erosion is associated with a more established, memory-biased and clonally expanded adaptive T cell response, whereas rupture reflects a more abrupt thrombo-inflammatory milieu with less evidence of preceding local adaptive immune enrichment. Indeed, histopathological analyses often reveal thrombus organization and remodeling in eroded plaques, suggesting that the initial endothelial injury can occur up to a week before thrombus formation and clinical presentation(70, 71). This subacute lesion-thrombus interface could favor recruitment, retention, or reactivation of pre-existing antigen-experienced effector and memory T cells. As an alternative, non-mutually exclusive explanation, it has been speculated(70) that T cells may crucially contribute to early plaque evolution in erosion by infiltrating nascent atherosclerotic lesions or predilection sites, where only small areas of endothelial cell loss occur, so-called microerosions(70). Repeated cycles of localized T cell–mediated endothelial injury and repair could then drive T cell activation and memory formation on the one hand, and a chronic healing response on the other hand, resulting in the deposition of excess collagen III and hyaluronan, as characteristically observed in advanced plaque erosion(70).

Contrasting functional T cell programs in erosion and rupture

T cell polarization within a local tissue environment is influenced by antigen-presentation, costimulatory signals, and the surrounding cytokine milieu. Under pro-inflammatory cues, $CD4^+$ T cells can adopt T_H1 or T_H1/T_H17 proinflammatory programs, predominantly releasing IFNγ and IL-17, which promote inflammatory cytokine release, myeloid activation and recruitment, and endothelial damage. Conversely, in a tolerogenic cytokine milieu, the same naïve precursors can

ACCEPTED MANUSCRIPT

Downloaded from academic.oup.com/cardiovascres/advance-article/doi/10.1093/cvr/cvag258/9005686 by guest on 03 November 2026

differentiate into protective T_{regs} that secrete IL-10 and TGF-β, restraining effector cells and favoring lesion stabilization(27).

The relative dominance of these opposing lineages, proinflammatory T_H1 and T_H1/T_H17 cells in rupture versus T_{regs} in erosion, provides a mechanistic framework for understanding the distinct immune environments of these lesions. In rupture, $CD4^+$ and $CD8^+$ pathway enrichment in inflammatory response, cytokine production, type II interferon signaling, leukocyte chemotaxis, and immune effector functions reflects an acute, proinflammatory activation, aligning with the relative predominance of T_H1 and T_H1/T_H17 cells and fewer culprit-proximal T_{regs}. This constellation is consistent with a poorly regulated immune surge triggered by sudden cap fracture. Supporting this, elevated peripheral T_{reg} abundance in rupture without corresponding local accumulation could represent a systemic regulatory response that fails to achieve effective lesion-level control due to impaired homing or retention of T_{regs} at the site, leaving the local environment dominated by proinflammatory responses, fostering unchecked vascular injury and rapid thrombus propagation. In erosion, enrichment of pathways linked to integrin-mediated adhesion, active proliferation, and extracellular matrix interaction in both $CD4^+$ and $CD8^+$ T cells suggests that T cells are not merely passively trapped but display transcriptional features compatible with local engagement at the lesion-thrombus interface. This milieu also favors the accumulation of T_{regs}, which may restrain local inflammation and cytotoxicity, thus limiting tissue damage. However, the concurrent presence of proliferating $CD8^+$ effector cells with cytolytic potential suggests that, despite regulatory influences, $CD8^+$ T cell-mediated endothelial injury can persist, sustaining thrombus growth and lesion progression. Collectively, these data suggest that plaque erosion may involve chronic, antigen-experienced immune responses balancing regulatory and cytotoxic forces, whereas rupture reflects an acute, unrestrained proinflammatory activation with less evidence of local immune regulation.

ACCEPTED MANUSCRIPT

Downloaded from academic.oup.com/cardiovascres/advance-article/doi/10.1093/cvr/cvag258/9005686 by guest on 03 November 2026

Implications for therapy and translation

The observation of fundamentally distinct adaptive immune trajectories and phenotypes in plaque erosion versus rupture underscores both the potential and the need for future studies to establish plaque-morphology–guided immunomodulatory and anti-inflammatory therapies in ACS. The predominant T_H1 and T_H1/T_H17 T cell response in rupture suggests that anti-inflammatory therapies modulating cytokine pathways such as IFNγ- or IL-17 blockers could help reduce unchecked inflammation and limit thrombus expansion after cap rupture.

In contrast, the oligoclonal T cell response in erosion calls for more specific interventions: Alongside other potential strategies addressing key pathways in erosion pathogenesis, such as TLR2 blockade on neutrophils and HYAL2 inhibition(20), therapies aimed at enhancing T_{reg} recruitment or function, or modulating cytotoxic T cell activity could be explored as potential approaches to reduce ongoing endothelial injury and curb thrombus progression in erosion-prone lesions. The LILACS phase I/II trial in patients with ischemic heart disease and ACS showed that short-term subcutaneous low-dose IL-2 induces selective T_{reg} expansion even in the context of advanced atherosclerosis(72). This was supported by a recent study that showed clonal expansion of effector T_{regs} with an enhanced immunoregulatory phenotype in coronary artery disease patients in response to low-dose IL-2(73). The ongoing IVORY trial is actively assessing the impact of low-dose IL-2 on vascular inflammation post-ACS(74). Given the distinct immune profile in ACS due to plaque erosion, it is plausible -though unproven- that these patients could benefit from T_{reg}-directed therapies such as low-dose IL-2. Moreover, the pronounced accumulation of clonally expanded, cytotoxic $CD8^+$ T cells at the culprit site indicates that targeting cytotoxic T cell activity may represent an additional strategy to reduce endothelial injury and constrain thrombus formation. Agents targeting T cell effector pathways, such as granzyme B inhibitors or inhibitors of perforin-mediated cytotoxicity, could offer novel approaches to directly protect the endothelium. For example, *in vitro* and animal studies demonstrate that the granzyme

ACCEPTED MANUSCRIPT

Downloaded from academic.oup.com/cardiovascres/advance-article/doi/10.1093/cvr/cvag258/9005686 by guest on 03 November 2026

B inhibitor SerpinA3N effectively attenuates granzyme B-mediated tissue damage, including preservation of collagen structure and reduced vascular injury (75, 76).

Limitations of the study

This study has several important limitations. First, PBMC preparations inherently exclude granulocytes such as neutrophils, which play a central role in plaque erosion. Dedicated studies focusing on neutrophil programming in erosion, including neutrophil–T cell crosstalk, are warranted. Second, our analyses are restricted to the liquid phase, specifically blood aspirated from the proximal coronary microenvironment, without direct investigation of the plaque tissue itself. Moreover, although matched peripheral samples were available for flow cytometry and allowed us to distinguish several culprit-proximal from systemic immune alterations, CITE-seq and paired TCR-seq were performed only on culprit-proximal coronary blood. Thus, transcriptional and clonal differences identified by single-cell multiomics cannot be fully separated from systemic immune variation at the same molecular resolution. Third, our single-cell approach does not allow the determination of T cell antigen specificity, which remains technically challenging in humans due to limitations of current TCR sequencing and epitope mapping methods (27). Thus, we cannot identify the specific antigens driving T cell activation or expansion in plaque erosion and plaque rupture. Similarly, while we mapped expanded clonotypes to a curated CVD-TCR database, this analysis does not prove antigen specificity, does not establish a breach of immune tolerance, and does not allow us to determine whether clonally enriched T cells preceded, contributed to, or followed plaque erosion. Fourth, because samples were collected only at the time of the acute event, we lack information on the inflammatory status at baseline or before symptom onset and have merely a speculative understanding of the processes leading to disease manifestations. We thus cannot definitively establish whether the observed immune profiles represent pre-existing

ACCEPTED MANUSCRIPT

Downloaded from academic.oup.com/cardiovascres/advance-article/doi/10.1093/cvr/cvag258/9005686 by guest on 03 November 2026

conditions contributing to plaque destabilization or are reactive changes occurring during the acute phase. Consequently, while our data are consistent with subacute or chronic antigen-driven T cell activation in erosion, we cannot determine if T cell recruitment and activation occur secondary to endothelial damage, or if they precede it. The observed differences between erosion and rupture should therefore be interpreted as phenotype-associated immune responses rather than as evidence that these immune features caused either plaque phenotype. Fifth, although OCT image acquisition and analysis were performed using a rigorously standardized methodology with dual independent core-lab adjudication, OCT inherently remains an imaging-based surrogate rather than a histopathological assessment. Consequently, despite expert interpretation and validated criteria, misclassification of plaque phenotypes cannot be entirely excluded. Finally, the sample size for our single-cell analyses was relatively small, which limits statistical power and generalizability. Nevertheless, the consistency of our findings was validated by multiparameter flow cytometry in a larger cohort. Taken together, these datasets constitute the most comprehensive immune profiling of plaque erosion and rupture reported to date.

Funding

This study was supported by a CRU grant from the Berlin Institute of Health (BIH) and the German Centre for Cardiovascular Research (DZHK; FKZ: 81Z2100202) to DML. Furthermore, an educational grant from Abbott Vascular (formerly: St. Jude Medical) provided OCT imaging to DML. TG was supported by a Walter Benjamin fellowship by the German Research Foundation (DFG; GE 3588/1-1) and is supported by the DFG, Project ID: 390649896, EXC 2026; the DFG, SFB 1531 - Projectnumber 456687919, and the DZHK (German Centre for Cardiovascular Research), funding code: 81X3200132. HH is supported by the Walter Benjamin Fellowship of the DFG (HO 7496/1-2) and the American Heart Association Postdoctoral Fellowship (AHA

ACCEPTED MANUSCRIPT

Downloaded from academic.oup.com/cardiovascres/advance-article/doi/10.1093/cvr/cvag258/9005686 by guest on 03 November 2026

#26POST1563188). CW received a doctoral scholarship by DZHK. HW received funding from the DFG (GRK 2407: 360043781); SFB TRR259 (397484323 project A04 (together with SB) and A09 as well as project 535107899); the Center for Molecular Medicine Cologne; and the Neven-DuMont Foundation. NG received funding from the DFG through CRC/TRR 259 (grant 397484323, project A05), CRC 1774 (grant 556052979, projects B01 and S01), and grant 569468610 (GE 2217/4-1). CG acknowledges support from grants NIH/NHLBI R01HL153712 and the American Heart Association AHA 20SFRN35210252. DW holds a professorship for Cardiovascular Systems Immunology funded by the Else-Kröner-Fresenius Foundation. This work has received funding from the European Research Council (ERC) under the European Union's Horizon 2020 research and innovation program (grant agreement No 853425). This work was supported by the Koeln Fortune Program/Faculty of Medicine, University of Cologne.

Acknowledgements

We are thankful to Sabine Knüppel, Christine Allomba, and Kerstin Gohlke for their help with patient recruitment and biomaterial processing. We thank the physicians and other staff of the catheterization laboratory at Charité Campus Benjamin Franklin, including Carsten Skurk, MD; Arash Haghikia, MD; Thomas Wurster, MD; David Sinning, MD; Ursula Rauch-Kroehnert, MD; Georg Girke, MD; Georg Froehlich, MD, and Markus Reinthaler, MD. We are grateful to the staff of the Berlin Institute of Health (BIH). We would like to acknowledge the excellent cooperation with the Central Biobank Charité (ZeBanC), which was responsible for the storage and processing of some of the biological samples. We would like to thank the staff at OLINK proteomics, especially Leonhard Pollack, PhD. We gratefully acknowledge the support of the FACS Core Facility, University of Cologne, in particular Lena Schumacher and Christian Kukat, for their assistance with sorting PBMC samples. We would like to thank Katharina Tinaz for her technical expertise during sample preparation.

ACCEPTED MANUSCRIPT

Downloaded from academic.oup.com/cardiovascres/advance-article/doi/10.1093/cvr/cvag258/9005686 by guest on 03 November 2026

COI and disclosures

The authors declare no conflicts of interest and have no disclosures.

References

1. Bhatt DL, Lopes RD, Harrington RA. Diagnosis and Treatment of Acute Coronary Syndromes: A Review. Jama. 2022;327(7):662-75.
2. Cannon CP, Blazing MA, Giugliano RP, McCagg A, White JA, Theroux P, et al. Ezetimibe Added to Statin Therapy after Acute Coronary Syndromes. N Engl J Med. 2015;372(25):2387-97.
3. Sabatine MS, Giugliano RP, Keech AC, Honarpour N, Wiviott SD, Murphy SA, et al. Evolocumab and Clinical Outcomes in Patients with Cardiovascular Disease. N Engl J Med. 2017;376(18):1713-22.
4. Bonaca MP, Bhatt DL, Cohen M, Steg PG, Storey RF, Jensen EC, et al. Long-term use of ticagrelor in patients with prior myocardial infarction. N Engl J Med. 2015;372(19):1791-800.
5. Alexander JH, Lopes RD, James S, Kilaru R, He Y, Mohan P, et al. Apixaban with antiplatelet therapy after acute coronary syndrome. N Engl J Med. 2011;365(8):699-708.
6. Mega JL, Braunwald E, Wiviott SD, Bassand JP, Bhatt DL, Bode C, et al. Rivaroxaban in patients with a recent acute coronary syndrome. N Engl J Med. 2012;366(1):9-19.
7. Chiarito M, Cao D, Cannata F, Godino C, Lodigiani C, Ferrante G, et al. Direct Oral Anticoagulants in Addition to Antiplatelet Therapy for Secondary Prevention After Acute Coronary Syndromes: A Systematic Review and Meta-analysis. JAMA Cardiol. 2018;3(3):234-41.
8. Jernberg T, Hasvold P, Henriksson M, Hjelm H, Thuresson M, Janzon M. Cardiovascular risk in post-myocardial infarction patients: nationwide real world data demonstrate the importance of a long-term perspective. Eur Heart J. 2015;36(19):1163-70.
9. Steen DL, Khan I, Andrade K, Koumas A, Giugliano RP. Event Rates and Risk Factors for Recurrent Cardiovascular Events and Mortality in a Contemporary Post Acute Coronary Syndrome Population Representing 239 234 Patients During 2005 to 2018 in the United States. J Am Heart Assoc. 2022;11(9):e022198.
10. Libby P. Mechanisms of acute coronary syndromes and their implications for therapy. N Engl J Med. 2013;368(21):2004-13.
11. Libby P, Pasterkamp G. Requiem for the 'vulnerable plaque'. Eur Heart J. 2015;36(43):2984-7.
12. Libby P, Pasterkamp G, Crea F, Jang IK. Reassessing the Mechanisms of Acute Coronary Syndromes. Circ Res. 2019;124(1):150-60.

ACCEPTED MANUSCRIPT

Downloaded from academic.oup.com/cardiovascres/advance-article/doi/10.1093/cvr/cvag258/9005686 by guest on 03 November 2026

13. Jia H, Abtahian F, Aguirre AD, Lee S, Chia S, Lowe H, et al. In vivo diagnosis of plaque erosion and calcified nodule in patients with acute coronary syndrome by intravascular optical coherence tomography. J Am Coll Cardiol. 2013;62(19):1748-58.
14. Leistner DM, Kränkel N, Meteva D, Abdelwahed YS, Seppelt C, Stähli BE, et al. Differential immunological signature at the culprit site distinguishes acute coronary syndrome with intact from acute coronary syndrome with ruptured fibrous cap: results from the prospective translational OPTICO-ACS study. Eur Heart J. 2020;41(37):3549-60.
15. Farb A, Burke AP, Tang AL, Liang TY, Mannan P, Smialek J, et al. Coronary plaque erosion without rupture into a lipid core. A frequent cause of coronary thrombosis in sudden coronary death. Circulation. 1996;93(7):1354-63.
16. Ferrante G, Nakano M, Prati F, Niccoli G, Mallus MT, Ramazzotti V, et al. High levels of systemic myeloperoxidase are associated with coronary plaque erosion in patients with acute coronary syndromes: a clinicopathological study. Circulation. 2010;122(24):2505-13.
17. Quillard T, Araújo HA, Franck G, Shvartz E, Sukhova G, Libby P. TLR2 and neutrophils potentiate endothelial stress, apoptosis and detachment: implications for superficial erosion. Eur Heart J. 2015;36(22):1394-404.
18. Gerhardt T, Seppelt C, Abdelwahed YS, Meteva D, Wolfram C, Stapmanns P, et al. Culprit plaque morphology determines inflammatory risk and clinical outcomes in acute coronary syndrome. Eur Heart J. 2023;44(38):3911-25.
19. Ruggio A, Pedicino D, Flego D, Vergallo R, Severino A, Lucci C, et al. Correlation between CD4(+)CD28(null) T lymphocytes, regulatory T cells and plaque rupture: An Optical Coherence Tomography study in Acute Coronary Syndromes. Int J Cardiol. 2019;276:289-92.
20. Meteva D, Vinci R, Seppelt C, Abdelwahed YS, Pedicino D, Nelles G, et al. Toll-like receptor 2, hyaluronan, and neutrophils play a key role in plaque erosion: the OPTICO-ACS study. Eur Heart J. 2023;44(38):3892-907.
21. Vergallo R, Papafaklis MI, D'Amario D, Michalis LK, Crea F, Porto I. Coronary plaque erosion developing in an area of high endothelial shear stress: insights from serial optical coherence tomography imaging. Coron Artery Dis. 2019;30(1):74-5.
22. Nakajima A, Sugiyama T, Araki M, Seegers LM, Dey D, McNulty I, et al. Plaque Rupture, Compared With Plaque Erosion, Is Associated With a Higher Level of Pancoronary Inflammation. JACC Cardiovasc Imaging. 2022;15(5):828-39.
23. Seppelt C, Abdelwahed YS, Meteva D, Nelles G, Stähli BE, Erbay A, et al. Coronary microevaginations characterize culprit plaques and their inflammatory microenvironment in a subtype of acute coronary syndrome with intact fibrous cap: results from the prospective translational OPTICO-ACS study. Eur Heart J Cardiovasc Imaging. 2024;25(2):175-84.
24. Yamamoto E, Yonetsu T, Kakuta T, Soeda T, Saito Y, Yan BP, et al. Clinical and Laboratory Predictors for Plaque Erosion in Patients With Acute Coronary Syndromes. J Am Heart Assoc. 2019;8(21):e012322.
25. Niccoli G, Montone RA, Di Vito L, Gramegna M, Refaat H, Scalone G, et al. Plaque rupture and intact fibrous cap assessed by optical coherence tomography portend different outcomes in patients with acute coronary syndrome. Eur Heart J. 2015;36(22):1377-84.
26. Liuzzo G, Pedicino D, Vinci R, Crea F. CD8 lymphocytes and plaque erosion: a new piece in the jigsaw. Eur Heart J. 2020;41(37):3561-3.
27. Saigusa R, Winkels H, Ley K. T cell subsets and functions in atherosclerosis. Nat Rev Cardiol. 2020;17(7):387-401.

ACCEPTED MANUSCRIPT

Downloaded from academic.oup.com/cardiovascres/advance-article/doi/10.1093/cvr/cvag258/9005686 by guest on 03 November 2026

28. Wolf D, Gerhardt T, Winkels H, Michel NA, Pramod AB, Ghosheh Y, et al. Pathogenic Autoimmunity in Atherosclerosis Evolves From Initially Protective Apolipoprotein B(100)-Reactive CD4(+) T-Regulatory Cells. Circulation. 2020;142(13):1279-93.
29. Roffi M, Patrono C, Collet JP, Mueller C, Valgimigli M, Andreotti F, et al. 2015 ESC Guidelines for the management of acute coronary syndromes in patients presenting without persistent ST-segment elevation: Task Force for the Management of Acute Coronary Syndromes in Patients Presenting without Persistent ST-Segment Elevation of the European Society of Cardiology (ESC). Eur Heart J. 2016;37(3):267-315.
30. Ibanez B, James S, Agewall S, Antunes MJ, Bucciarelli-Ducci C, Bueno H, et al. 2017 ESC Guidelines for the management of acute myocardial infarction in patients presenting with ST-segment elevation: The Task Force for the management of acute myocardial infarction in patients presenting with ST-segment elevation of the European Society of Cardiology (ESC). Eur Heart J. 2018;39(2):119-77.
31. Stoeckius M, Hafemeister C, Stephenson W, Houck-Loomis B, Chattopadhyay PK, Swerdlow H, et al. Simultaneous epitope and transcriptome measurement in single cells. Nat Methods. 2017;14(9):865-8.
32. McGinnis CS, Murrow LM, Gartner ZJ. DoubletFinder: Doublet Detection in Single-Cell RNA Sequencing Data Using Artificial Nearest Neighbors. Cell Systems. 2019;8(4):329-37.e4.
33. Mulè MP, Martins AJ, Tsang JS. Normalizing and denoising protein expression data from droplet-based single cell profiling. Nat Commun. 2022;13(1):2099.
34. Amrute JM, Jung I-H, Yamawaki T, Lin W-L, Bredemeyer A, Diekmann J, et al. Targeting modulated vascular smooth muscle cells in atherosclerosis via FAP-directed immunotherapy. Science. 2026;392(6793):eadx1736.
35. Fernandez DM, Rahman AH, Fernandez NF, Chudnovskiy A, Amir E-aD, Amadori L, et al. Single-cell immune landscape of human atherosclerotic plaques. Nature Medicine. 2019;25(10):1576-88.
36. Horstmann H, Michel NA, Sheng X, Hansen S, Lindau A, Pfeil K, et al. Cross-species single-cell RNA sequencing reveals divergent phenotypes and activation states of adaptive immunity in human carotid and experimental murine atherosclerosis. Cardiovasc Res. 2024;120(14):1713-26.
37. Barcia Durán JG, Das D, Gildea M, Amadori L, Gourvest M, Kaur R, et al. Immune checkpoint landscape of human atherosclerosis and influence of cardiometabolic factors. Nature Cardiovascular Research. 2024;3(12):1482-502.
38. van Blokland IV, Oelen R, Groot HE, Benjamins JW, Pekayvaz K, Losert C, et al. Single-Cell Dissection of the Immune Response After Acute Myocardial Infarction. Circulation: Genomic and Precision Medicine. 2024;17(3):e004374.
39. Qian J, Gao Y, Lai Y, Ye Z, Yao Y, Ding K, et al. Single-Cell RNA Sequencing of Peripheral Blood Mononuclear Cells From Acute Myocardial Infarction. Frontiers in Immunology. 2022;Volume 13 - 2022.
40. Gavish A, Tyler M, Greenwald AC, Hoefflin R, Simkin D, Tschernichovsky R, et al. Hallmarks of transcriptional intratumour heterogeneity across a thousand tumours. Nature. 2023;618(7965):598-606.
41. Barkley D, Moncada R, Pour M, Liberman DA, Dryg I, Werba G, et al. Cancer cell states recur across tumor types and form specific interactions with the tumor microenvironment. Nat Genet. 2022;54(8):1192-201.

ACCEPTED MANUSCRIPT

Downloaded from academic.oup.com/cardiovascres/advance-article/doi/10.1093/cvr/cvag258/9005686 by guest on 03 November 2026

42. Yerly L, Andreatta M, Garnica J, Domizio JD, Gilliet M, Carmona SJ, et al. Wounding triggers invasive progression in human basal cell carcinoma. bioRxiv. 2024:2024.05.31.596823.
43. Korotkevich G, Sukhov V, Budin N, Shpak B, Artyomov MN, Sergushichev A. Fast gene set enrichment analysis. bioRxiv. 2021:060012.
44. Hao Y, Hao S, Andersen-Nissen E, Mauck WM, 3rd, Zheng S, Butler A, et al. Integrated analysis of multimodal single-cell data. Cell. 2021;184(13):3573-87.e29.
45. Robinson MD, McCarthy DJ, Smyth GK. edgeR: a Bioconductor package for differential expression analysis of digital gene expression data. Bioinformatics. 2010;26(1):139-40.
46. Squair JW, Gautier M, Kathe C, Anderson MA, James ND, Hutson TH, et al. Confronting false discoveries in single-cell differential expression. Nat Commun. 2021;12(1):5692.
47. Zhou Y, Zhou B, Pache L, Chang M, Khodabakhshi AH, Tanaseichuk O, et al. Metascape provides a biologist-oriented resource for the analysis of systems-level datasets. Nat Commun. 2019;10(1):1523.
48. Zhang EY, Kong KF, Altman A. The yin and yang of protein kinase C-theta (PKCθ): a novel drug target for selective immunosuppression. Adv Pharmacol. 2013;66:267-312.
49. Zhang Y, Liu Q, Yang S, Liao Q. CD58 Immunobiology at a Glance. Front Immunol. 2021;12:705260.
50. Ross SH, Cantrell DA. Signaling and Function of Interleukin-2 in T Lymphocytes. Annu Rev Immunol. 2018;36:411-33.
51. Oh SA, Li MO. TGF-β: guardian of T cell function. J Immunol. 2013;191(8):3973-9.
52. Cruikshank W, Little F. lnterleukin-16: the ins and outs of regulating T-cell activation. Crit Rev Immunol. 2008;28(6):467-83.
53. Cichocki F, Miller JS. Promoting T and NK cell attack: preserving tumor MICA/B by vaccines. Cell Res. 2022;32(11):961-2.
54. Ramji DP, Davies TS. Cytokines in atherosclerosis: Key players in all stages of disease and promising therapeutic targets. Cytokine Growth Factor Rev. 2015;26(6):673-85.
55. Galvan MD, Foreman DB, Zeng E, Tan JC, Bohlson SS. Complement component C1q regulates macrophage expression of Mer tyrosine kinase to promote clearance of apoptotic cells. J Immunol. 2012;188(8):3716-23.
56. Mullan KA, de Vrij N, Valkiers S, Meysman P. Current annotation strategies for T cell phenotyping of single-cell RNA-seq data. Front Immunol. 2023;14:1306169.
57. Poon MML, Caron DP, Wang Z, Wells SB, Chen D, Meng W, et al. Tissue adaptation and clonal segregation of human memory T cells in barrier sites. Nat Immunol. 2023;24(2):309-19.
58. Liu X, Gosline SJC, Pflieger LT, Wallet P, Iyer A, Guinney J, et al. Knowledge-based classification of fine-grained immune cell types in single-cell RNA-Seq data. Brief Bioinform. 2021;22(5).
59. Mohanta SK, Heron C, Klaus-Bergmann A, Horstmann H, Brakenhielm E, Giannarelli C, et al. Metabolic and Immune Crosstalk in Cardiovascular Disease. Circ Res. 2025;136(11):1433-53.
60. Feng X, Wang L, Zhou R, Zhou R, Chen L, Peng H, et al. Senescent immune cells accumulation promotes brown adipose tissue dysfunction during aging. Nature Communications. 2023;14(1):3208.

ACCEPTED MANUSCRIPT

Downloaded from academic.oup.com/cardiovascres/advance-article/doi/10.1093/cvr/cvag258/9005686 by guest on 03 November 2026

61. Hochnadel I, Hoenicke L, Petriv N, Suo H, Groebe L, Olijnik C, et al. In vivo RNAi screen and validation reveals Ngp, Hba-a1, and S100a8 as novel inhibitory targets on T lymphocytes in liver cancer. Frontiers in Immunology. 2025;Volume 16 - 2025.
62. Lee J, Kim H, Kim M, Yoon S, Lee S. Role of lymphoid lineage cells aberrantly expressing alarmins S100A8/A9 in determining the severity of COVID-19. Genes Genomics. 2023;45(3):337-46.
63. Oesinghaus L, Becker S, Vornholz L, Papalexi E, Pangallo J, Moinfar AA, et al. A single-cell cytokine dictionary of human peripheral blood. bioRxiv. 2025:2025.12.12.693897.
64. Türk L, Filippov I, Arnold C, Zaugg J, Tserel L, Kisand K, et al. Cytotoxic CD8(+) Temra cells show loss of chromatin accessibility at genes associated with T cell activation. Front Immunol. 2024;15:1285798.
65. Freuchet A, Roy P, Armstrong SS, Oliaeimotlagh M, Kumar S, Orecchioni M, et al. Identification of human exTreg cells as CD16+CD56+ cytotoxic CD4+ T cells. Nature Immunology. 2023;24(10):1748-61.
66. Richter L, Dias-Ferreira J, Campos Ramos G, Ashour D. T Cell Receptor Repertoires Across the Continuum of Vascular, Myocardial, and Age-Related Diseases. Immunological Reviews. 2026;339(1):e70125.
67. Virmani R, Burke AP, Farb A, Kolodgie FD. Pathology of the vulnerable plaque. J Am Coll Cardiol. 2006;47(8 Suppl):C13-8.
68. Ahmed ME, Leistner DM, Hakim D, Abdelwahed Y, Coskun AU, Maynard C, et al. Endothelial Shear Stress Metrics Associate With Proinflammatory Pathways at the Culprit Site of Coronary Erosion. JACC Basic Transl Sci. 2024;9(11):1269-83.
69. Horstmann H, Anto Michel N, Losert C, Abogunloko T, Peikert A, Hansen S, et al. Immunological risk identified by single-cell multi-omics and cardiovascular outcomes. Eur Heart J. 2026.
70. Lin S, Yu Y, Söderström L, Gisterå A. Erosion of the Atheroma: Wicked T Cells at the Culprit Site. Curr Atheroscler Rep. 2024;27(1):4.
71. Baaten C, Nagy M, Bergmeier W, Spronk HMH, van der Meijden PEJ. Platelet biology and function: plaque erosion vs. rupture. Eur Heart J. 2024;45(1):18-31.
72. Zhao TX, Sriranjan RS, Lu Y, Hubsch A, Kaloyirou F, Vamvaka E, et al. Low dose interleukin-2 in patients with stable ischaemic heart disease and acute coronary syndrome (LILACS). European Heart Journal. 2020;41(Supplement_2).
73. Case AG, O'Brien JW, Lu Y, Charlier FTW, Zhao X, Weng Y, et al. Low-dose interleukin-2 induces clonal expansion of BACH2-repressed effector regulatory T cells following acute coronary syndrome. Nat Cardiovasc Res. 2025;4(6):727-39.
74. Sriranjan R, Zhao TX, Tarkin J, Hubsch A, Helmy J, Vamvaka E, et al. Low-dose interleukin 2 for the reduction of vascular inflammation in acute coronary syndromes (IVORY): protocol and study rationale for a randomised, double-blind, placebo-controlled, phase II clinical trial. BMJ Open. 2022;12(10):e062602.
75. Ang LS, Boivin WA, Williams SJ, Zhao H, Abraham T, Carmine-Simmen K, et al. Serpina3n attenuates granzyme B-mediated decorin cleavage and rupture in a murine model of aortic aneurysm. Cell Death Dis. 2011;2(9):e209.
76. Huang H, Mu Y, Li S. The biological function of Serpinb9 and Serpinb9-based therapy. Front Immunol. 2024;15:1422113.

ACCEPTED MANUSCRIPT

Downloaded from academic.oup.com/cardiovascres/advance-article/doi/10.1093/cvr/cvag258/9005686 by guest on 03 November 2026

Figure Legends

Figure 1: Flowchart of patient selection and sample allocation for flow cytometry, and CITE- and TCR-seq in the OPTICO-ACS study. ACS, acute coronary syndrome; CL, culprit lesion; OCT, optical coherence tomography; CITE-seq, cellular indexing of transcriptomes and epitopes by sequencing; CV risk factors, cardiovascular risk factors; TCR-seq, T cell receptor sequencing.

Figure 2: Paired culprit-proximal immunophenotyping reveals divergent T-cell and proteomic signatures in plaque erosion and rupture. (**a**) Study workflow. Patients with acute coronary syndrome (ACS) underwent intracoronary optical coherence tomography (OCT) to assess culprit lesion morphology. Blood was collected from the culprit vessel directly proximal to the ACS-causing lesion (culprit-proximal immune compartment) and the distal radial artery (systemic inflammatory baseline); the culprit ratio (CR) was defined as the culprit-proximal divided by the systemic measurement, indexing local coronary immune-cell enrichment. All samples underwent flow cytometry (n=21 erosion, n=49 rupture), with a matched proximal subset selected for CITE-seq and TCR-seq (n=8 vs. 8). The lower panel shows the timing of sampling relative to angiography, OCT, and PCI. (**b**) Gating hierarchy used to define T-cell differentiation states: $CD4^+$ or $CD8^+$ T cells were split by CD45RA into $CD45RA^+$ (Naïve, TEMRA) and $CD45RA^-$ (central memory, TCM; effector memory, TEM) compartments. (**c**) Proximal memory T cells: $CD4^+$ and $CD8^+$ TEM/TCM as a proportion of $CD4^+$ or $CD8^+$ T cells (top) and their culprit ratios (bottom), in erosion versus rupture (n=16–19 erosion, 39–43 rupture). (**d**) Proximal $CD4^+$ T cell subsets as proportions of total $CD4^+$ T cells (n= 16–18 erosion, 34–42 rupture). (**e**) Culprit ratios of the T cell subsets in (d), shown as a radar plot (n=15–18 erosion, 38–42 rupture). (**f**) Ranked proximal coronary plasma protein abundance (log2 fold change, erosion versus rupture) measured with a

ACCEPTED MANUSCRIPT

Downloaded from academic.oup.com/cardiovascres/advance-article/doi/10.1093/cvr/cvag258/9005686 by guest on 03 November 2026

targeted Olink Explore 384 inflammation panel (n=19 erosion, 12 rupture); each dot is one protein, with selected erosion- and rupture-associated proteins labelled. For statistical analyses, normality was assessed by Shapiro–Wilk test; independent t-tests were used for normally distributed data and Mann–Whitney U tests otherwise. The schematic in (a) was created in BioRender.com under agreement number HU29Y28TKQ. TFH= T-follicular helper cell, TH= T-helper, Treg= regulatory T cell.

Figure 3: Single-cell multiomics uncovers distinct T cell activation and functional programs in erosion and rupture ACS. (**a**) Atherosclerotic plaque similarity. For each donor, a pseudobulk transcriptional profile was correlated (Spearman) against six independent scRNA-seq reference cohorts (n = 151 donors), and a plaque similarity index was derived as the mean correlation to a combined plaque reference (carotid + coronary). Box plots compare peripheral blood (healthy controls, ACS) with culprit-proximal aspirates (rupture, erosion); groups were compared by Wilcoxon rank-sum test. (**b**) Non-negative matrix factorization (NMF) was applied to the RNA assay of the CITE-seq data to detect transcriptional metaprograms. The heatmap displays Jaccard similarity indices among robust NMF programs based on their top 50 genes; programs are clustered and grouped into six metaprograms (MP1–MP6), numbered and labelled with representative genes. (**c**) The two differentially enriched metaprograms, MP3 (Memory T cell Nexus) and MP6 (Cytotoxic T cell Nexus), are shown as rank plots of module enrichment score split by condition (erosion, brown; rupture, blue); statistical significance was tested using the Mann–Whitney U test. (**d**) Single-cell modalities from 16 CITE-seq datasets were integrated using variance-stabilizing transformation (VST) and Seurat's anchor-based integration, and RNA and ADT assays were analyzed jointly by weighted nearest neighbor (WNN) analysis. After dimensionality reduction, 96,391 single-cell transcriptomes were projected in UMAP space; SLM clustering identified distinct leukocyte clusters grouped into meta-clusters based on hematopoietic lineage and activation status. (**e**) UMAP projections split by condition (erosion, rupture), showing

ACCEPTED MANUSCRIPT

Downloaded from academic.oup.com/cardiovascres/advance-article/doi/10.1093/cvr/cvag258/9005686 by guest on 03 November 2026

no apparent batch effect between groups. (**f**) Cell-type proportions (% of total leukocyte transcriptomes per sample) are shown as donut plots by condition. (**g**) Volcano plots display differentially expressed genes (DEGs) in $CD4^+$ and $CD8^+$ T cells between erosion and rupture, identified by patient-level pseudobulking within the LIBRA framework using edgeR and likelihood-ratio testing; selected genes are labelled. (**h**) Pathway enrichment analysis of significantly regulated genes in the $CD4^+$ and $CD8^+$ T cell compartments was performed using Metascape. Bubble size indicates the percentage of genes recovered per pathway, the y-axis shows enrichment score, and the x-axis denotes $-\log_{10}$(p-value); colour indicates the condition in which each pathway was enriched. Samples from n = 16 patients were included. Metaprogram enrichment between erosion and rupture was compared using the Mann–Whitney U test; DEGs were identified by patient-level pseudobulking followed by edgeR likelihood-ratio testing; Metascape p-values were calculated using a cumulative hypergeometric distribution and reported as $-\log_{10}$ values.

Figure 4. Cytokine response profiling reveals divergent T cell states in rupture and erosion. (a) Workflow schematic. Single-cell transcriptomic profiles from rupture and erosion lesions (discovery cohort, n=8 vs. n=8) were used for cytokine interaction motif modeling and cytokine response inference using huCIRA (human Cytokine Response Analysis), a GSEA-based enrichment method built on a reference atlas of cytokine-induced transcriptional responses across PBMC populations. This identified candidate cytokines predicted to be differentially active between conditions (e.g., IFN-γ, IL-1β, IL-27 in rupture; IL-10, IL-27, TSLP in erosion). Predictions were experimentally validated by isolating PBMCs from the proximal coronary segment, stimulating in vitro alongside a paired unstimulated baseline, and quantifying cytokine-producing T cells by flow cytometry. (b) Heatmap of huCIRA enrichment scores across cytokines (columns) and PBMC populations (rows), comparing rupture versus erosion. Blue indicates enrichment in

ACCEPTED MANUSCRIPT

Downloaded from academic.oup.com/cardiovascres/advance-article/doi/10.1093/cvr/cvag258/9005686 by guest on 03 November 2026

rupture; brown indicates enrichment in erosion; scale capped at ±2. (c–e) GSEA rank plots of huCIRA normalized enrichment scores (NES) for cytokines predicted to act on (c) $CD4^+$ TEM/TCM, (d) $CD8^+$ TEM/TCM, and (e) T_{reg} populations, ranked separately by enrichment in rupture (blue, left) and erosion (brown, right). Top-ranked cytokines for each condition are listed alongside. (f–h) Experimental validation of top huCIRA-predicted cytokines by flow cytometry in paired unstimulated versus stimulated PBMCs from the proximal coronary segment (erosion n=19-23, rupture n=49-51). (f) IL-2^+ $CD4^+$ TEM/TCM in erosion (left) and rupture (middle) patients, and log2(fold-change) of stimulated IL-2 compared between groups (right). (g) IFN-γ^+ $CD8^+$ TEM/TCM, same layout. (h) IL-10^+ Treg, same layout. P-values for paired unstimulated-vs-stimulated comparisons are from paired t-tests; between-group log2(fold-change) comparisons are from Mann-Whitney U tests. Each dot represents one patient; lines connect paired unstimulated/stimulated samples from the same individual.

Figure 5: Enhanced clonal expansion of T cells in plaque erosion. (a) $CD4^+$ and $CD8^+$ T cells were subset from the integrated Seurat object and subclustered using ADT expression data. A panel of 33 T cell-specific ADT markers was selected as variable features. To account for batch effects, the dataset was split, and singular value decomposition (SVD) was applied, followed by reciprocal latent semantic indexing (rLSI)–based integration. Clustering was performed using the Leiden algorithm (resolution = 0.6) on the integrated SVD reduction and visualized using UMAP. (**b)** DSB-normalized ADT expression levels used for annotation are shown as violin plots. **(c)** Cell-type proportions (% of total leukocyte transcriptomes per sample) are shown as stacked bar plots, grouped by condition. **(d)** Odds ratios (ORs) comparing the frequency of each T cell cluster between rupture and erosion were calculated by constructing 2x2 contingency tables per cluster (presence vs. absence in rupture vs. erosion), followed by OR estimation using Fisher's exact test. Resulting p-values were adjusted for multiple comparisons across clusters using the Benjamini–Hochberg procedure (false discovery rate, FDR). **(e)** TCR metadata was integrated

ACCEPTED MANUSCRIPT

Downloaded from academic.oup.com/cardiovascres/advance-article/doi/10.1093/cvr/cvag258/9005686 by guest on 03 November 2026

with the Seurat object using the scRepertoire package, annotating each T cell with its clonal frequency and clonal size. Clonal expansion was visualized by overlaying these metrics onto the UMAP projections. **(f)** Clonal occupancy across annotated T cell clusters and conditions (erosion vs. rupture) is depicted as stacked bar charts. **(g)** Ranked gene enrichment analysis of differentially expressed genes in oligoclonal versus non-oligoclonal T cells, shown separately for $CD8^+$ T cells (top row) and $CD4^+$ T cells (bottom row). For each T cell subset, genes enriched in oligoclonal cells from Rupture patients (left panels) and Erosion patients (right panels) are ranked by average log2 fold change. Canonical genes in each condition are labelled. (**h)** Pathway enrichment analysis of oligoclonal $CD8^+$ T cells (top) and oligoclonal $CD4^+$ T cells (bottom), comparing Erosion and Rupture patients. Each bubble represents one enriched pathway; x-axis indicates statistical significance ($-\log_{10}$ p-value), y-axis indicates enrichment score, and bubble size reflects the number of genes in the pathway. (**i**) Transcription factor (TF) activity was inferred using pySCENIC applied to the single-cell transcriptomic data. For each TF, a regulon was constructed based on co-expression with predicted target genes, and per-cell regulon activity was quantified as an AUC score. Delta AUC represents the difference in mean regulon activity between oligoclonal T cells from patients with plaque erosion versus plaque rupture (Delta AUC = AUC_erosion − AUC_rupture), calculated separately for $CD8^+$ (top) and $CD4^+$ (bottom) T cell compartments. TFs are ordered by Delta AUC magnitude.

Figure 6. TCR profiling reveals clonal restriction and disease-linked clonotype sharing in erosion. (a) Schematic of the analytical workflow. Three complementary TCR analyses were performed: clonal sharing between patients, repertoire diversity quantification, and CDR3β sequence mapping to the CVD-TCR public database (Richter et al., 2026). **(b)** Circos plots showing shared TCR clonotypes between individual patients, for the TRA chain (left) and TRB chain (right). Each outer arc represents one patient, colored by disease group. Arc width is

ACCEPTED MANUSCRIPT

Downloaded from academic.oup.com/cardiovascres/advance-article/doi/10.1093/cvr/cvag258/9005686 by guest on 03 November 2026

proportional to the number of unique expanded clonotypes detected in that patient. Ribbons connect patients sharing identical clonotypes and are colored according to the disease groups involved. Only expanded clonotypes (clone size ≥ 2) are included, consistent with the expansion threshold applied throughout the manuscript. **(c)** Hierarchical clustering of TCR repertoires by sample was performed using the Ward.D2 linkage method based on clonal similarity. **(d)** Clonal diversity estimated by Chao1 indices, assessing the full repertoire (TRA and TRB combined) as well as individual chains separately. **(e)** Binary heatmap showing the presence (grey) or absence (white) of CDR3β sequences (columns, n = 19) shared between OPTICO patients and the CVD-TCR public database (Richter et al., 2026) across disease categories (rows). Column annotations indicate OPTICO group membership. Numerical annotations show the total number of CVD-TCR database categories (N Pathologies) and independent published studies (N Studies) in which each sequence was previously reported. **(f)** Jaccard similarity index between OPTICO TCR repertoires and each CVD-TCR database category, shown for Erosion and Rupture. The Jaccard index quantifies the proportion of CDR3β sequences shared between an OPTICO group and a CVD category relative to their union, providing a normalized measure of repertoire overlap. **(g)** Per-patient frequency-weighted CDR3β overlap with the three CVD-TCR categories showing the strongest differential signal: Atherosclerosis-related (left), Ischemic cardiac damage (centre), and exTregs from Atherosclerosis (right). The overlap metric is defined as the sum of cell frequencies carrying a CDR3β sequence also found in the respective CVD-TCR category, divided by total patient cell count, expressed as a percentage. This weighting accounts for clonal expansion, such that an expanded shared clone contributes proportionally more than a singleton. Each dot represents one patient (Erosion n = 8, Rupture n = 8). Horizontal bar indicates the median. P-values from two-sided Wilcoxon rank-sum test. The schematic in (a) was created in BioRender under the agreement number *AM29Y8G5XN.*

ACCEPTED MANUSCRIPT

Downloaded from academic.oup.com/cardiovascres/advance-article/doi/10.1093/cvr/cvag258/9005686 by guest on 03 November 2026

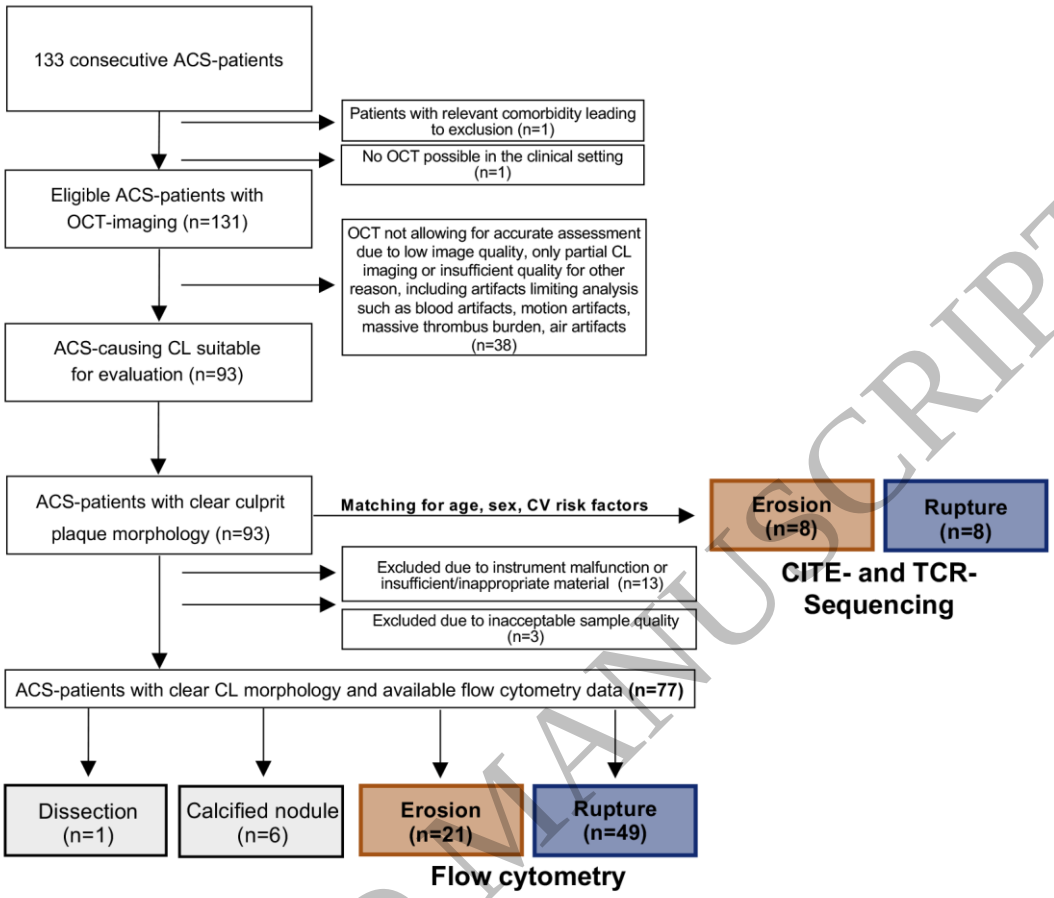


Figure 1
145x122 mm (x DPI)

ACCEPTED MANUSCRIPT

Downloaded from academic.oup.com/cardiovascres/advance-article/doi/10.1093/cvr/cvag258/9005686 by guest on 03 November 2026

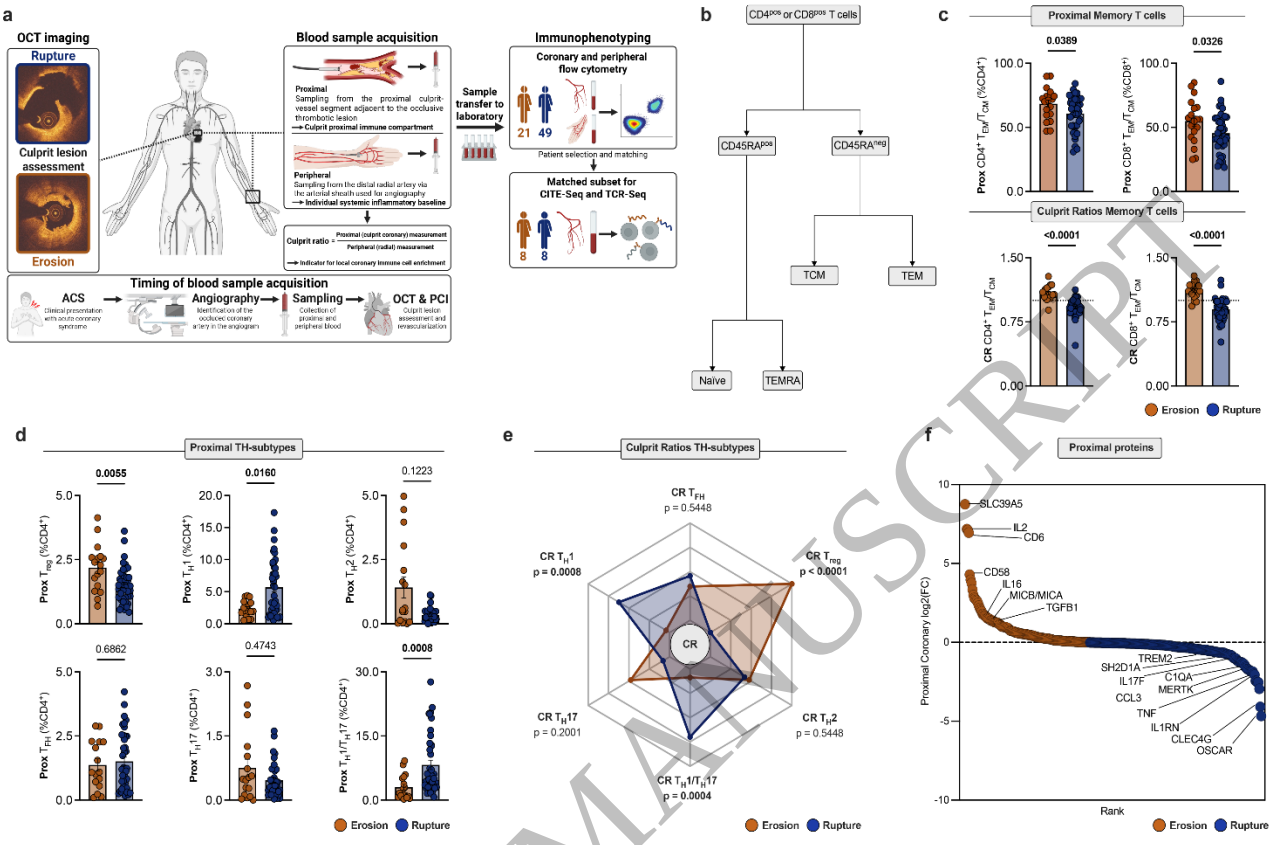


Figure 2
522x331 mm (x DPI)

ACCEPTED MANUSCRIPT

Downloaded from academic.oup.com/cardiovascres/advance-article/doi/10.1093/cvr/cvag258/9005686 by guest on 03 November 2026

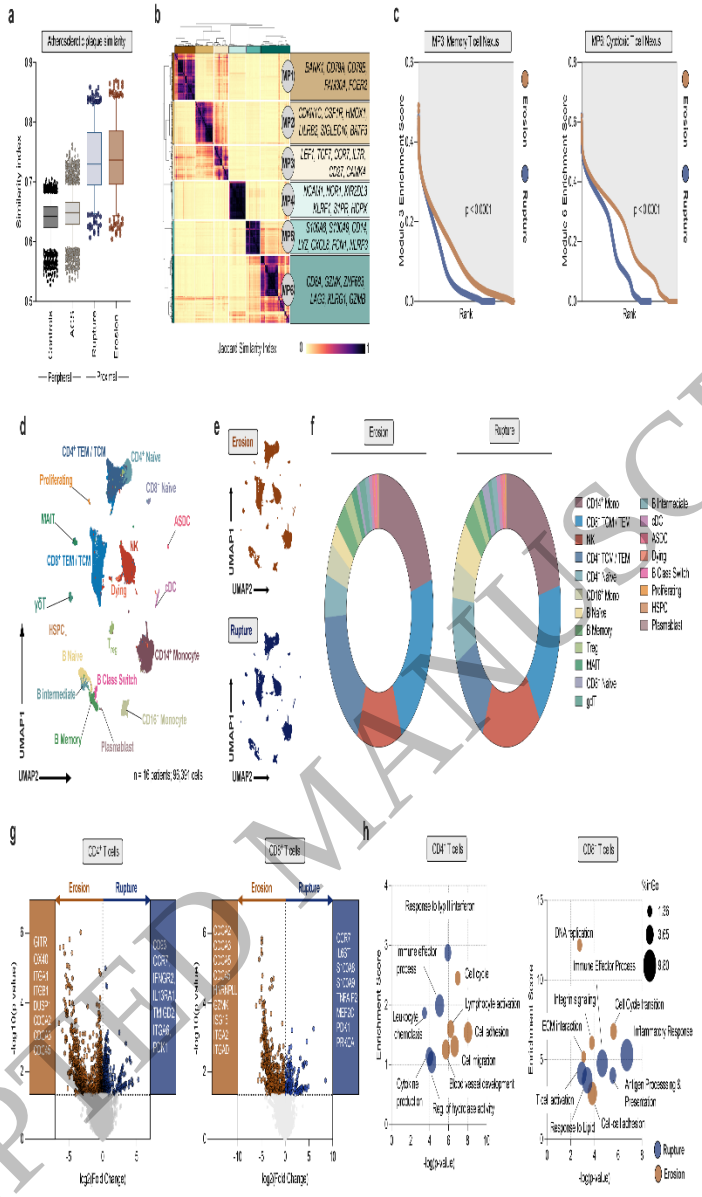


Figure 3
508x350 mm (x DPI)

ACCEPTED MANUSCRIPT

Downloaded from academic.oup.com/cardiovascres/advance-article/doi/10.1093/cvr/cvag258/9005686 by guest on 03 November 2026

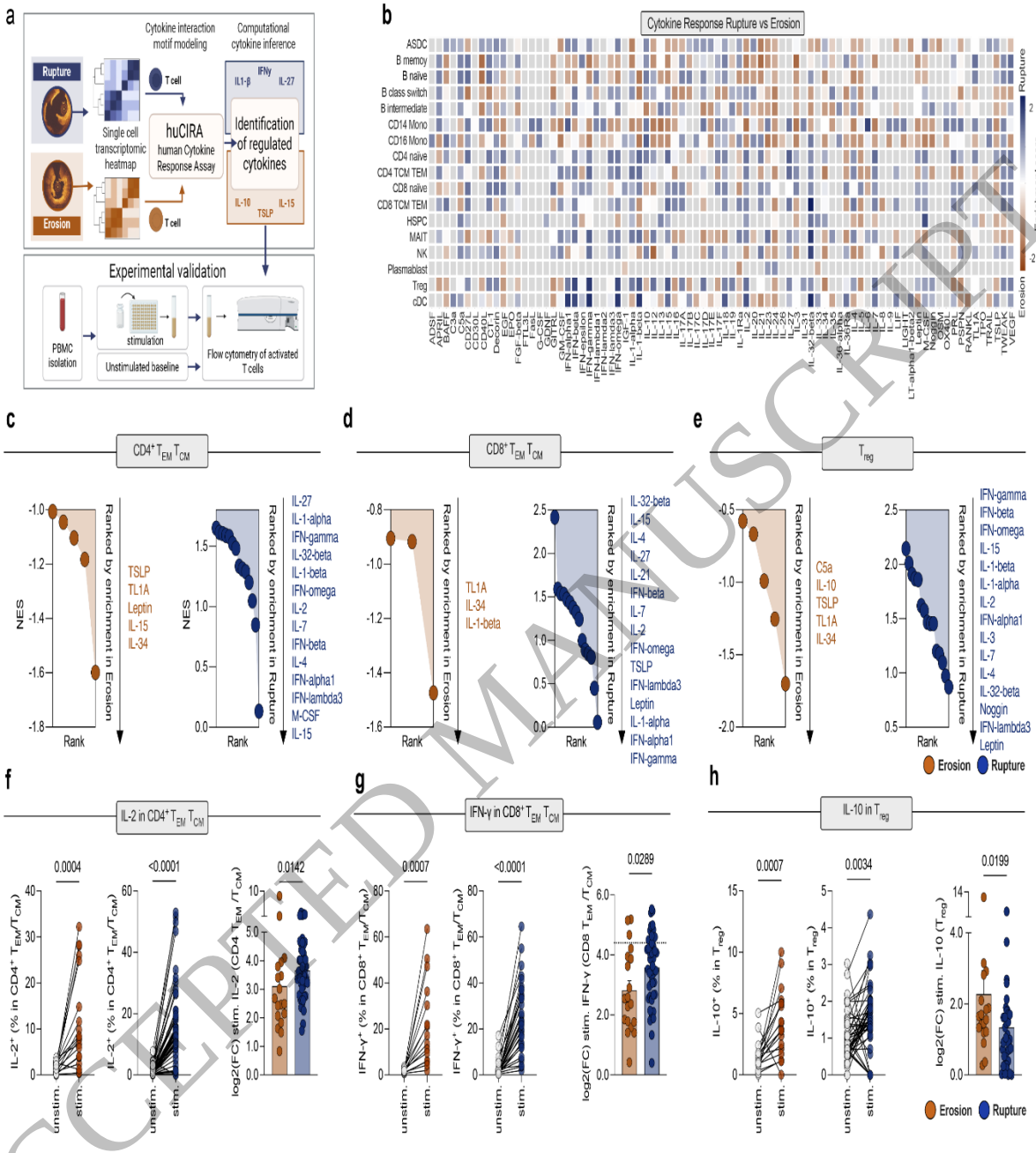


Figure 4
488x318 mm (x DPI)

ACCEPTED MANUSCRIPT

Downloaded from academic.oup.com/cardiovascres/advance-article/doi/10.1093/cvr/cvag258/9005686 by guest on 03 November 2026

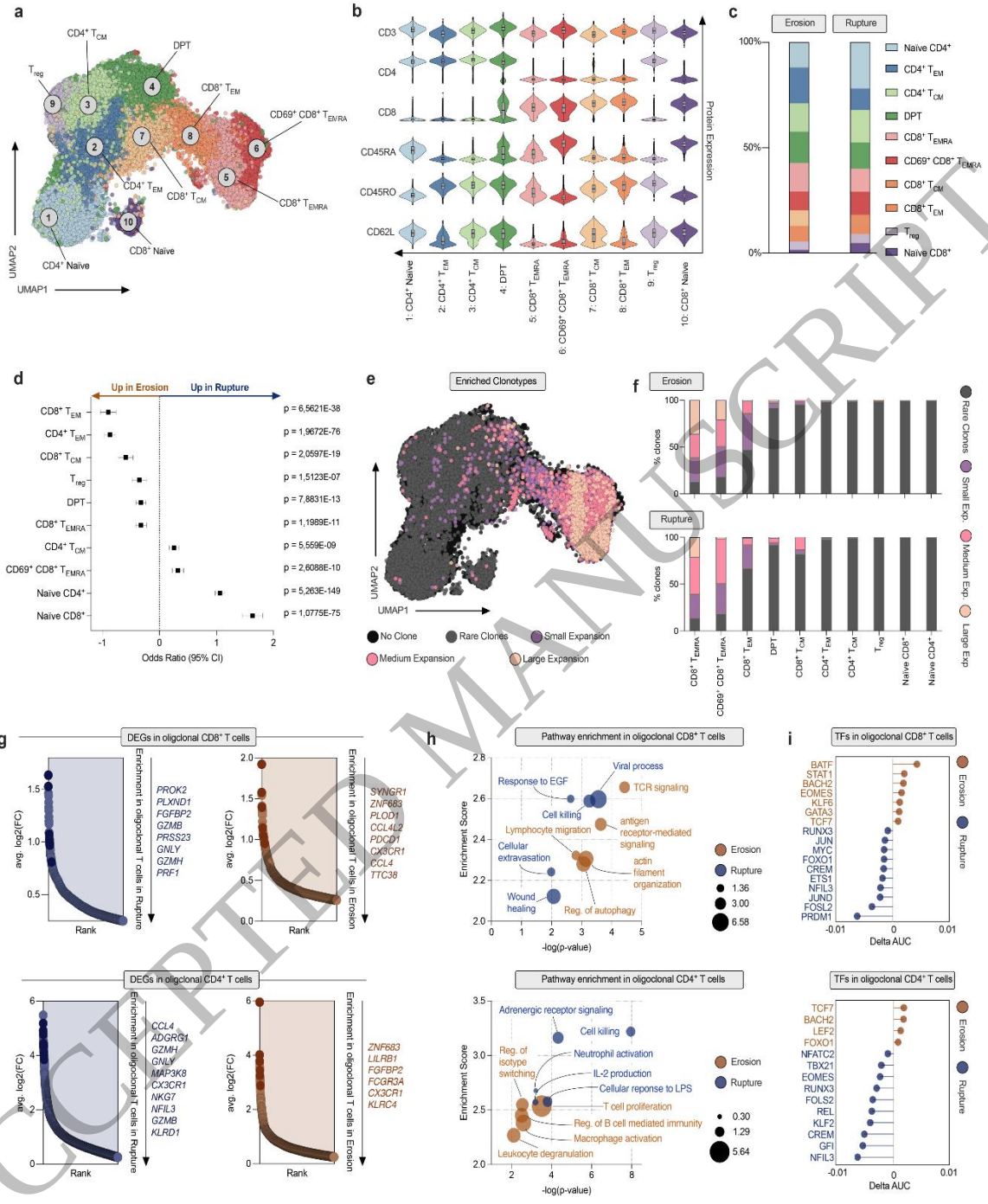


Figure 5
464x512 mm (x DPI)

ACCEPTED MANUSCRIPT

Downloaded from academic.oup.com/cardiovascres/advance-article/doi/10.1093/cvr/cvag258/9005686 by guest on 03 November 2026

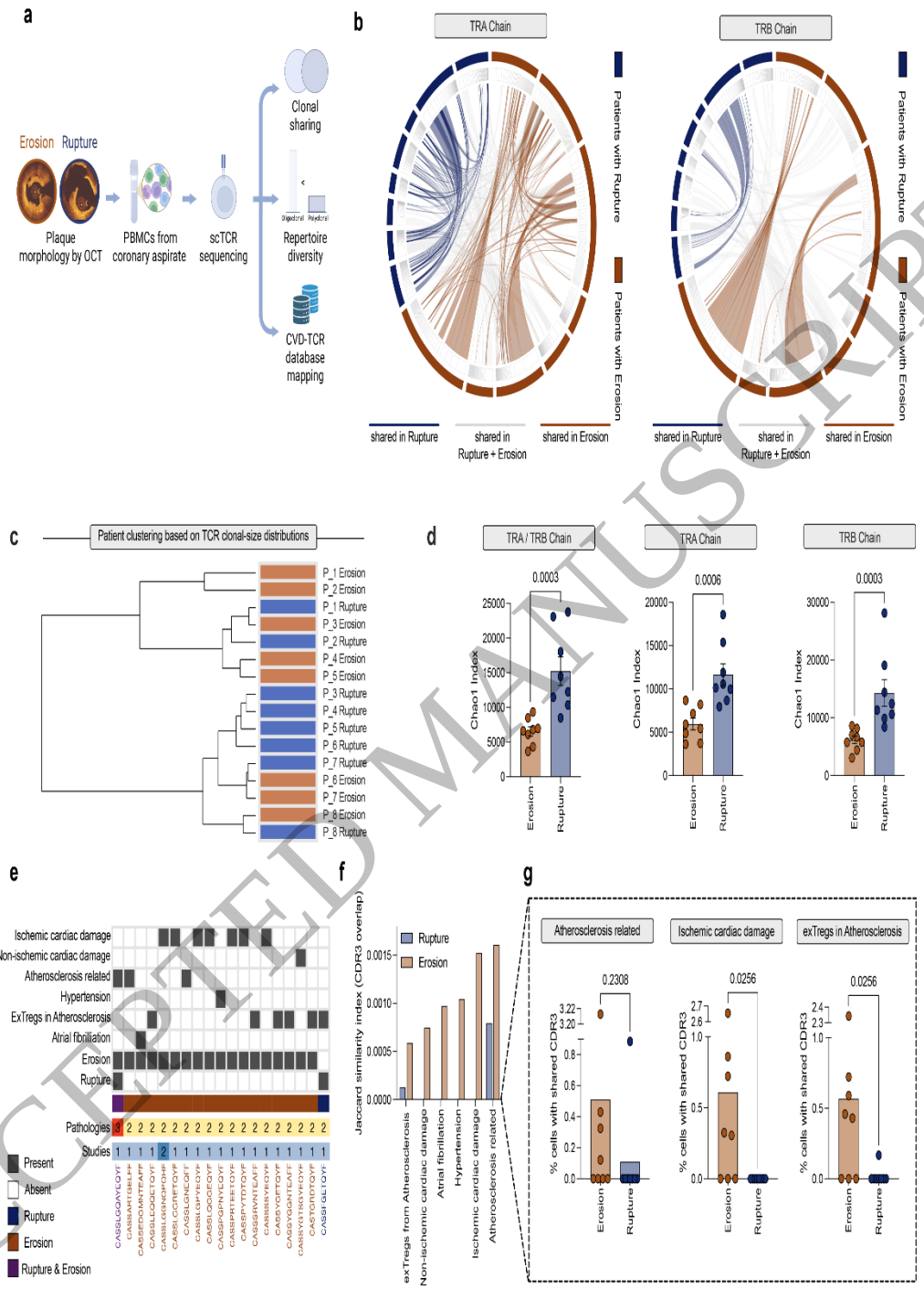


Figure 6
457x382 mm (x DPI)

ACCEPTED MANUSCRIPT

Downloaded from academic.oup.com/cardiovascres/advance-article/doi/10.1093/cvr/cvag258/9005686 by guest on 03 November 2026